QATAR UNIVERSITY

COLLEGE OF ENGINEERING

# NOVEL PROCESS FOR DESIGNING TOPOLOGY OPTIMIZED FEMORAL STEMS PRINTABLE BY METAL ADDITIVE MANUFACTURING

BY

TAREK SALAHELDIN MAHMOUD MOHAMED SHABAN

A Thesis Submitted to

the Faculty of the College of Engineering

in Partial Fulfillment of the Requirements for the Degree of

Masters of Science in Mechanical Engineering

June 2019

# COMMITTEE PAGE

The members of the Committee approve the Thesis of Tarek Salaheldin Mahmoud Mohamed Shaban defended on 01/04/2019.

_____

Prof. Dr. Faris Tarlochan
Thesis/Dissertation Supervisor

Approved:

_____

Prof. Dr. Abdelmagid Hamouda, Dean, College of Engineering

# ABSTRACT

SHABAN, TAREK, S., Masters: April: 2019, Masters of Science in Mechanical Engineering

Title: Novel Process for Designing Topology Optimized Femoral Stems Printable by Metal Additive Manufacturing

Supervisor of Thesis: Faris, Tarlochan.

Total hip arthroplasty faces an issue of the high cost and risks of revision surgeries. Studies show that more than 50% of the revision surgeries are the consequence of the aseptic loosening of the implant. The cause of the loosening is the bone resorption during the bone remodeling due to poor load transfer to the bone because of the stiff metal used for the implant. The aim of this work is illustrating a novel process of designing topology optimized femoral stems printable by additive manufacturing to increase the load transfer. The proposed manual penalization process is used to produce the required stems followed by a multiple simulations process to select the optimum stem extraction iso-surface threshold value. The results show printable stems that increased the strain energy in the bone by 20% and had better micromotions uniform distribution resulting in more uniform bone growth.

# DEDICATION

*I dedicate this work to my father Salaheldin and my mother Abeer, my sister and best friend Shaden and my friends, especially my close friends Ahmed Shalaby and Tasneem Al-Mansy. A very special thanks and gratitude to my sister and best friend Shaden They were all always there charging me with whatever I needed all the time 24/7.*

# ACKNOWLEDGMENTS

I would like to express my sincere gratitude to my supervisor Dr. Faris Tarlochan for supporting and supervising my work and for making the supervision more of a fellowship into work journey. I would like to thank Eng. Sami Al Khatib and Dr. Hassan Mehboob for the provided technical support in my work a very warm thanks. In addition to my college in the program supporting technically as well, Eng. Nouman Al Qwasmi.

# TABLE OF CONTENTS

# LIST OF TABLES

# List of Figures

# NOMENCLATURE

**BW:** the load used for optimization is body weight load

**WL:** the load used for optimization is walking load

**BWT:** Post-Optimization simulation done by applying body weight load

**WLT:** Post-Optimization simulation done by applying walking load

**Ti:** Stands for Ti-6Al-4V alloy

**Co:** Stands for Co-Cr-Mo alloy

# CHAPTER 1 : INTRODUCTION

## 1.1. Background

Total hip arthroplasty is a medical procedure made to restore the function of the hip joint that is injured during an accident or no longer functioning due to osteoarthritis and osteoporosis that are common in elderly people (Perets et al., 2018) (Stibolt et al., 2018). The operation includes adding a femoral stem that is implanted in the femur bone and a plastic bio material cup that is inserted in the hip bone itself (Sandhu, 2015). The femoral stem has two parts, one is the ball joint connected to the hip bone responsible for the movement and the other is the stem that is implanted in the femur bone.

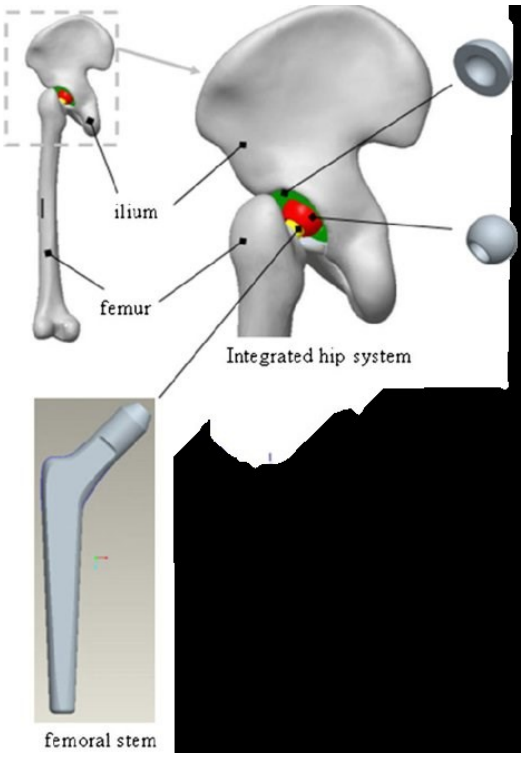


Figure 1 - Femoral stem composition (Li, Li, Lian, Guo, & Jin, 2010)

The significance of the stem being designed and used is due to the expected rates of the total number of operations globally to reach 4.5 million by 2050 increasing from 1.26 million in 1990 (Veronese & Maggi, 2018). To reduce the number of surgeries, the revision surgeries should be considered as in the UK alone, by 2016, there were more than 85000 revision surgeries more than 50% of them was due to aspect loosening (NJR, 2017). This is in addition to the risks and the costs associated with the revision surgeries as they are risky due to the change of the bone structure to weaker and the attachment of the implant in the bone (Grisez, Calkins, & Dietz, 2017) (Ong, Lau, Suggs, Kurtz, & Manley, 2010). It was found out for a study by Medicare Program that the costs of revision surgeries are of too high cost for the program and with low and poor outcome to the patient and thus it is required to focus on selecting improved implants in order to benefit the patient and reduce the risks and costs associated with the revision (Koenig, Feng, He, & Nguyen, 2018).

3D metal printing (also known as metal additive manufacturing) is evolving very quickly to the point that now it is being used by some of the large medical implant manufacturers, it was used in the early phases of development as a prototyping tool but now it has evolved. After speaking to the sales representative of Biomet implants in Qatar, Biomet a large implant manufacturer actually uses metal 3D printing for printing the femoral stems for some patients who fail to find their size of a suitable stem from the available off-shelf stems. The company made a special department for what they call Patient-Matched Implants (PMI) specific for patients who cannot easily find matched components to suit them (Zimmer Biomet, 2019). In addition to other medical companies obtaining the FDA approval for the use of 3D metal printing for other

medical implants are proves of the future of using 3D metal printing for many other implants ("FDA approval for 3D printed titanium implant," 2016) ("FDA approval for 3D printed titanium cranial plate," 2016).

To produce the required femoral stems to increase the load transfer to the bone this requires increasing the strain energy in the bone, requiring to reduce the strain energy in the stem (Alkhatib et al., 2019)(Oshkour et al., 2015). To achieve this, the tool of Topology Optimization will serve the need. The tool removes material to create voids inside a part/structure to make a new part while maintaining a certain set number of constrains to achieve a set objective function (W. Zhang, Zhou, & Zhu, 2017). The concern facing topology optimization is the printability of the designed products out of it (Mass & Amir, 2018). This thesis will suggest a process to optimize a femoral stem and convert it to a fully printable stem as the expected outcome from topology optimization software is a material density distribution including elements with relative density (density ratio not a full solid not a full void, similar to a material of a different properties) and these elements cannot be printed using additive manufacturing machines (Chang, Chen, Huang, & Hsu, 2012).

## 1.2. Problem statement

Aseptic loosening which is the cause of 50% of revision surgeries is due to the stiffness mismatch between the bone and the implant, a phenomena named stress shielding (X. Wang et al., 2016). The implant having a stiffness of around 110 GPa if made from titanium alloy, 200 if made from Cobalt chromium alloy and the bone on the other side having 17 GPa for the cortical bone(X. Wang et al., 2016) (Takumi et al., 2015), this large difference results in the stem holding the load of the body without transferring it to the bone which cause bone resorption according to bone remodeling

theory (Perrella, Fraldi, Esposito, Cowin, & Cutolo, 2009) (Chang et al., 2012). The problem is now in design a femoral stem that can transform the load from the hip bone to the femur bone thus maintaining the femur intact as much as possible by minimizing the bone resorption (Huiskes, Weinans, van Rietbergen, & Rietbergen, 1992). This can be done by using the optimization tool to increase the strain energy in the bone by reducing the strain energy in the femoral stems, as the increase of the strain energy enhances and motivates the bone growth process (G Robling & H Turner, 2009) (Alkhatib et al., 2019) (Oshkour et al., 2013).

In addition to making the stem as close as possible from the outer shape and coatings to the currently available stems to not require intensive research about the bio compatibility and body acceptance for it and it can be printed using the 3D metal printers that many companies are adapting as mentioned earlier.

### 1.3. Objectives

To achieve 3D printable femoral stems using topology optimization tool to reduce the stem stiffness in order to increase strain energy in the femur bone.

### 1.4. Structure of thesis

This thesis includes 5 chapters in total.

- The first introduction chapter gives a brief about the background of the problem and showing the significance of the issue and stating the objective of the study.
- Followed by a literature review chapter listing information about the hip and femur bone, remodeling theory and the forces applied on them.
- The third chapter includes the methodology used, starting from the suggested process of this work, the finite element model, the optimization model and the design of experiment followed.

- The fourth chapter includes the results divided in four subsections, the final optimized stems, the micromotions of the post-optimization simulations, the strain energy transfer results and the predictions of the maximum porosities achievable using the calculated factor of safety.

Followed by the conclusion and the references.

# CHAPTER 2 : Literature Review

## 2.1. Total Hip Arthroplasty

### *2.1.1. Hip Joint and Bone*

The hip bone is the lower bone of the body that is responsible for connecting both of the hips to the upper body (See Next Figure). The hip joint is the connection point between the femur bone and the hip bone where it has six degrees of freedom and connected through a cup and ball joint (See the second next Figure).

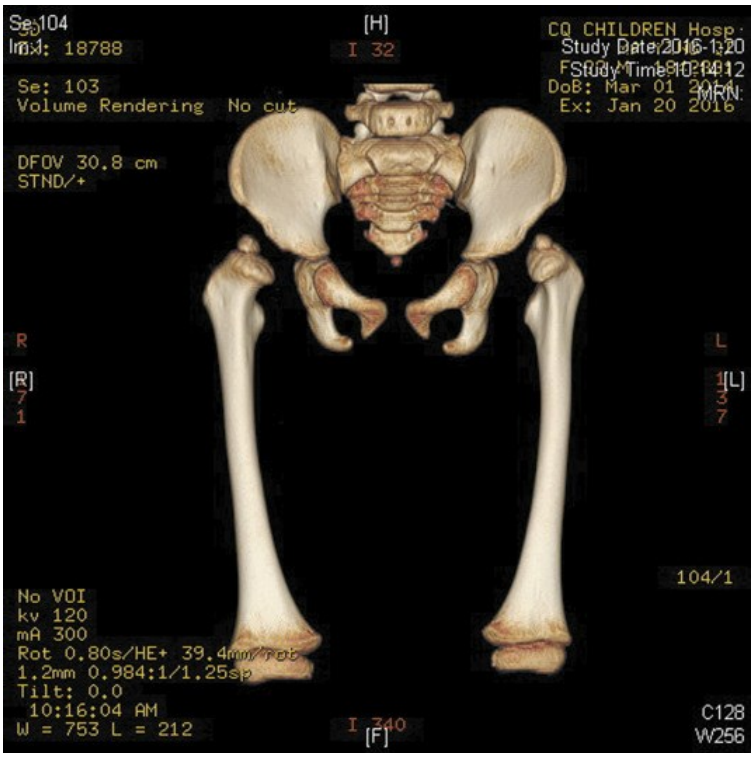


Figure 2 - Hip Bone top and two femur bones left and right bottom (J. Chen et al., 2018)

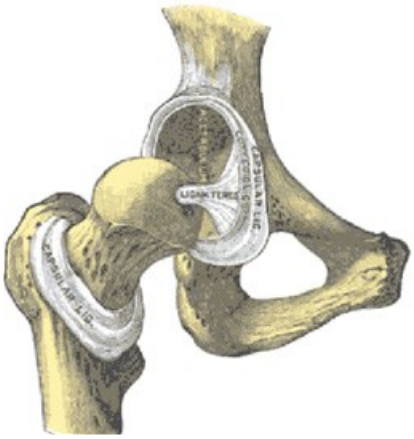

Figure 3 - Hip Joint, showing the femur bone left side with ball and hip bone top right (Mattei, Di Puccio, Piccigallo, & Ciulli, 2011)

### *2.1.2. Force on the Hip Joint*

The forces on any joint in the body and all tests are usually done in a fatigue cycle in what is known as gait cycles. For simplicity in this thesis, two of the loads will only be considered and for computational power and time limits, a static test will only be considered as the focus of this thesis is on the process of producing printable topology optimized stems. The two loads considered are from daily routine: standing load which is considered to be a point load by (335% of the body weight) 3000N on the femur ball, this is corresponds for the total body weight load applied during daily routine activities and is used for the beginning of load application during a gait cycle as mentioned by Bergmann, Deuretzbacher, Heller, Graichen, & Rohlmann, 2001) and walking loads that vary between 203 and 233% of the body weight given average body weight around 850 N (Bergmann, Deuretzbacher, Heller, Graichen, & Rohlmann, 2001). The exact value of forces used for the simulation can be found in chapter 5.

### *2.1.3. Bone Remodeling Theory*

The nature of the bone and the human body in general is to be adaptable to the nature. The bone as a living tissue is no different. It adjusts itself to reduce its mass either internally or externally based on the stress level being applied on it, internally would be by becoming more porous and externally by becoming thinner (Huiskes et al., 1992) (Ott, 2004). Despite of the improvements of stems over the past years, aseptic loosening is still the main failure reason of the implant at a rates of 15% in a time between 5-7 years after the surgery for cement-less stems (Dayton & Incavo, 2005).

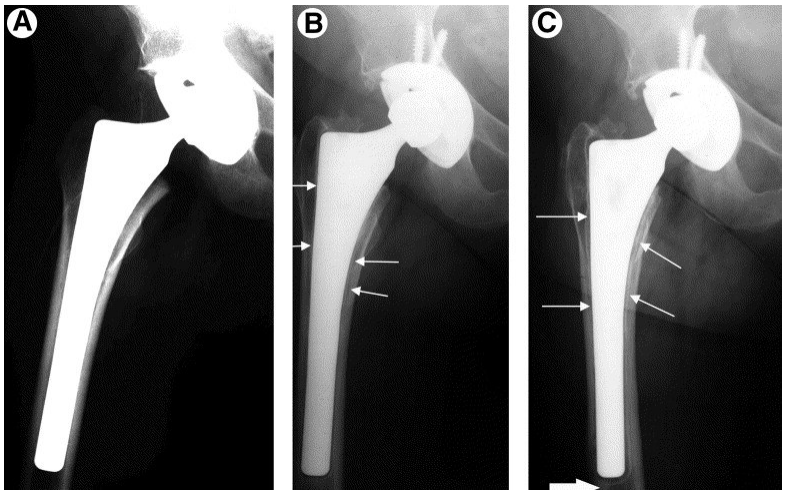


Figure 4 - Stem Aseptic Loosening, starting from A after implant direct, B after 3 years and C after 5 years (Dayton & Incavo, 2005)

## 2.2. Femoral Stems

### *2.2.1. Materials Used*

Currently the witnessed in the literature that there are two materials being used for femoral stems, Titanium alloy Ti-6Al-4V and Cobalt Chrome Molybdenum alloy Co-Cr-Mo with Ti-6Al-4V is the most commonly used nowadays (Colic et al., 2016) (K. B. Hazlehurst, 2014) (K. Hazlehurst, Wang, & Stanford, 2013). The use of the titanium allow is due to the less stiffness of the cobalt chrome alloy (K. Hazlehurst et al., 2013).

### *2.2.2. Femoral Stem Types*

There are different ways of categorizing stems, by the shape of the stem if it is one piece called the Monoblock stem inserted directly in the femur and the modular consists of two pieces one large one goes into the whole femur and is connected to the main stem that is slightly similar in shape with the Monoblock (Nadeau & Garbuz, 2016) (Grisez et al., 2017). The modular stem is usually used in revision surgeries except for some very severe cases thus the Monoblock stem is the mainly used (Grisez et al., 2017).


Figure 5 - Monoblock Stem (Grisez et al., 2017)


Figure 6 - Modular Stem, where on the right side the distal part of the femur with the stem continuing to the femur bone end (Grisez et al., 2017)

The Monoblock stem is the one mostly used for the first time in total hip arthroplasty and it comes in different shapes and lengths based on the reason for the operation. The following figure shows some lengths and shapes from Zimmer Biomet manufacturer.

Figure 7 - Monoblock stem examples (Biomet, 2012)

### *2.2.3. Stem Fixations*

There are two types of stem fixations in the femur, cement and cement-less. The

cement-less depends on a press-fit technique to be implanted giving a shorter operation time and better stability (Gehrke, Citak, & Ohlmeier, 2019) (Stibolt et al., 2018). The cemented stem however is mentioned in some literature for having better long term results but overall the debate about which is better over the long term was found equal (Kim, Park, Kim, & Kim, 2016). It is important to mention the disadvantage of the cemented stems in the case of revision surgeries due to difficulties of removing the old stem (Vargas-Hernandez, Bingham, Hart, & Sierra, 2017) (Grisez et al., 2017). The trend in the surgeries nowadays is to use the cement-less due to less operation time, better stability and less recovery time (Gehrke et al., 2019) (Vargas-Hernandez et al., 2017).

## 2.3. Topology Optimization

### *2.3.1. Introduction*

There are three types of optimization for parts/structures application, size optimization, shape optimization and topology optimization with the latest being the most sophisticated (Tian et al., 2019). The latest, topology optimization is a numerical tool for designing structures and parts with the best performance (K. Zhang, Cheng, & Xu, 2019). It works by removing material from a certain selected region to achieve a shape of the part that achieves the objective function and made to satisfy the set constrains. The following figure explains the algorithm behind it.

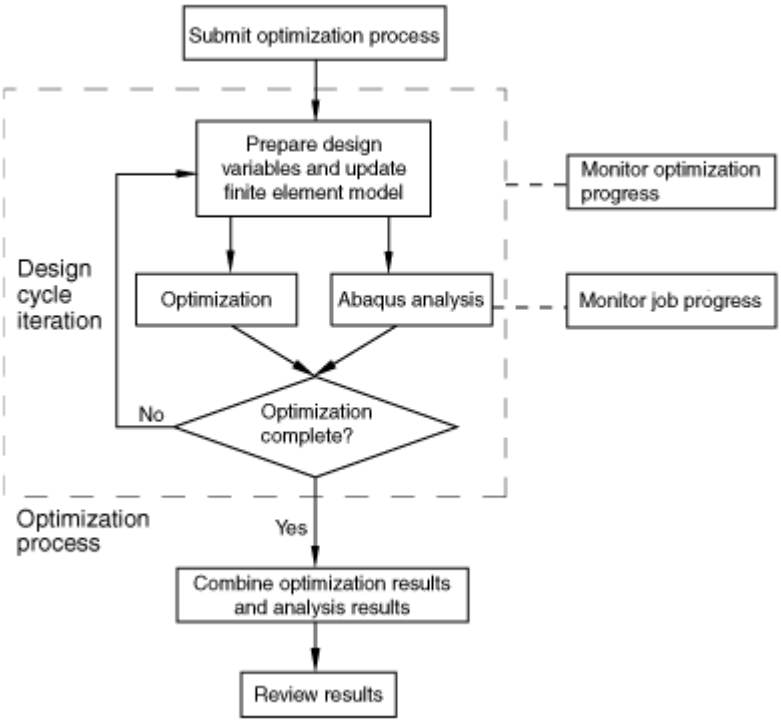


Figure 8 - Optimization Process

In the meantime, it is now a tool more than a process as there are multiple software with CAD user interface making it easier than it was in the early stages were it was done using codes and algorithms. The following figure shows as example of topology optimization to a beam supported from both ends with a uniform load applied on it similar to a simple bridge.

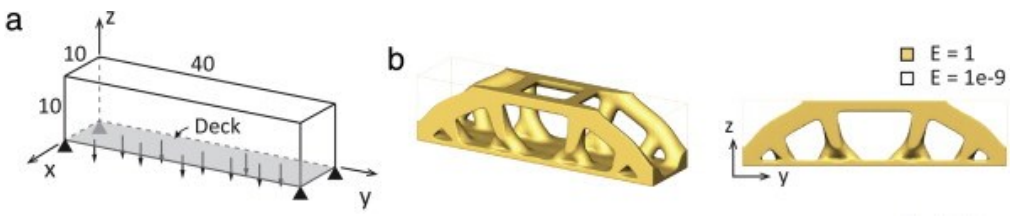


Figure 9 - Topology Optimization Example to a simple beam (Park & Sutradhar, 2015)

### *2.3.2. Algorithms/Methods*

There are many algorithms/methods used for topology optimization such as parametrized parameter set, evolutionary structural optimization (ESO) and solid isotropic material with penalization (SIMP) (S. Wang, Liu, Wang, Yan, & Deng, 2015) (Vasista & Tong, 2014). It has been proven that the most computationally efficient, close as possible to being able to be printed and the most used is the SIMP method and since the focus is to achieve printable stems then SIMP method will be used (Tian et al., 2019)(Gardan & Schneider, 2015) (Perrella et al., 2009) (K. Zhang et al., 2019) (S. Zhang, Le, Gain, & Norato, 2019) (Siva Rama Krishna, Mahesh, & Sateesh, 2017). The beneficial feature behind the SIMP is using the relative density (RD) concept of each element that has the value between 0-1 with 0 giving no element in the final optimized part and 1 is a full density element of the original material (K. Zhang et al., 2019). After setting all elements to RD of 1 in the first iteration, the simulation is done and the relative density distribution is changed across all elements in the changing region and the iterations continue. The penalization part comes in where some elements are removed for having such a very low RD while the rest remains.

### *2.3.3. Output of Optimization*

The final result of the optimization process is a part with most of the original elements with their new relative density, thus it is a map of the relative densities of the elements (K. Zhang et al., 2019) (Pasini, Tanzer, Rahimizadeh, Nourmohammadi, & Arabnejad, 2017). These elements are then extracted using the software, if the

extraction is direct, the part cannot be used as it contains only a relative density map, that means that not all elements are solid some of them has a relative density between 0 and 1, meaning its density relative to a real solid particle/element. During the extraction phase, a smoothing of the mesh is done by the software to make sure that the surface of the extracted mesh is smooth. This smoothing is done using a value called the iso-surface value which is a value between 0 and 1 again, it controls which element of the mesh is the element on the surface and evens the elements with reference to it by displacing the nodes on the surface making a new even surface based on the iso-surface value ("What is an optimization process?," n.d.), the value when increased makes that surface closer to the inside of the material and the opposite meaning more material when increased in the current case and less material when decreased. Extracting using the smoothing process with the iso-surface value will be used to benefit in the current work, this is to produced different porosities of the resultant optimized stem and to convert them to solid.

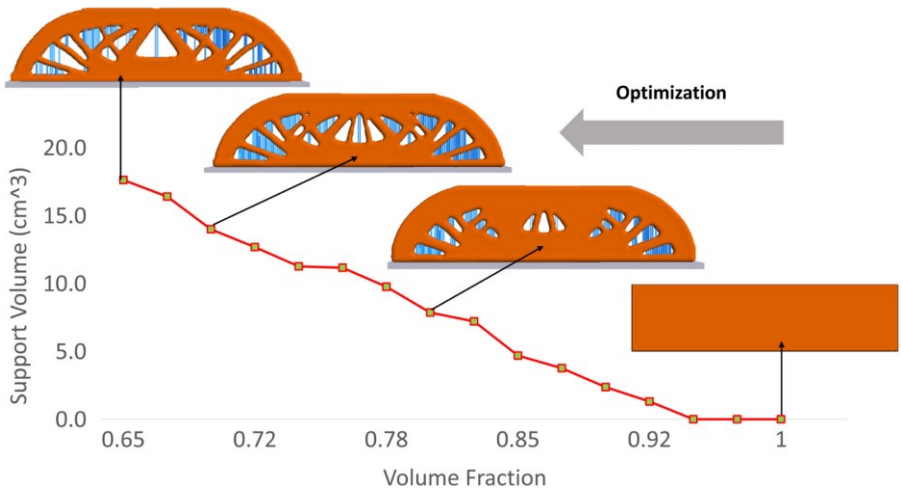


Figure 10 - Example of optimization output and Relative Density map (Mirzendehdel & Suresh, 2016)

### *2.3.4. Software Used*

There are many software for use in optimization most known are ABAQUS and ANSYS. ABAQUS uses the aid of TOSCA optimization codes and algorithms and ABAQUS 2017 is the one being used for this work.

## 2.4. Summary

- Fact 1: Aseptic loosening is the reason for more than 50% of revision surgeries.
- Fact 2: Aseptic loosening is due to poor load transfer to the bone.
- Fact 3: Topology optimization results in relative density element maps that cannot be printed using additive manufacturing.

# CHAPTER 3 : METHODOLOGY

## 3.1. Suggested Process for Optimized Printable Stems

### *3.1.1. Validated Model*

The first step would be to obtain and validate the model for the part being optimized, in the case of this thesis a femur bone with an implanted femoral stem were obtained from previous studies (Alkhatib et al., 2019) (Oshkour et al., 2015).The CADs were modified to meet some references in the literature for matching the results for validation and then the loads are set for a static test as required. The test should have the loads applied on the part set as in the validation reference.

### *3.1.2. Optimization*

The optimization is set in three stages, the first one is to select the region to have the elements removed from, where the software is allowed to change the relative density of the elements in this region. Then the objective function is set, the objective function is a scalar function in the simulation in the selected region to be minimize or maximized based on the requirement (Bruggi & Taliercio, 2014). The selection for this work was to minimize the strain energy in the internal region selected inside the femoral stem.

### *3.1.3. Manual Penalization*

As mentioned earlier, the result of the optimization is a map of the relative densities of the elements making the optimized part. The thesis work suggests a method using manual penalization (element removal) after the optimization is done and converting the result into a fully solid part where all elements are with relative density of 1 by using a threshold value for the iso-surface in the extraction process. The aim is to have multiple optimized stems with different porosities to study the

effect on the key results making the selection process of the required iso-surface value to achieve the desired key result. In order to get more stems it is suggested during the extraction phase to use the iso-surface value ranging between 0 and 1, changing the value between 0 and 1 results in having multiple stems with different porosities. Having a larger iso-surface value will result in having more material and visa versa meaning more porosity with smaller iso-surface value and less porosity with large iso-surface value. After optimization, there is a suggested iso-surface value giving only one stem, to have customized stems giving the required performance based on the key results, this requires having as many stems as possible simulated and this key result is measured and the data are plotted with respect to the porosity/iso-surface/threshold value and then the optimum value of the porosity/iso-surface-threshold is selected and the stem is extracted using this value. The process of extracting will be named manual penalization for ease of writing.

Multiple threshold values were selected and the results have been evaluated for performance and then the final selection of threshold for each part is selected. Previous work in the literature only smoothen out the resulting parts from the optimization and converted all elements to solid directly giving a part with more or less material than needed to achieve the key result aimed for. For the case of trying to increase the load transfer/strain energy transfer to the bone, having more material than needed will reduce the amount of energy transfer not giving the maximum possible as desired (Baharuddin et al., 2014). Optimization processes have already the penalization done during the process but it eliminates only elements with low relative density. After the extraction from the optimization is done, a conversion of the stems into parts that can be simulated was done using three software, the first one was Magics Materialize to

convert the stem into STL format as it is extracted as STL document from ABAQUS, then Solidworks to convert the STL file to STEP file to be imported in ABAQUS to do the post-optimization simulations.

### *3.1.4. The novelty in the process*

The following chart illustrates the three stages of the process:

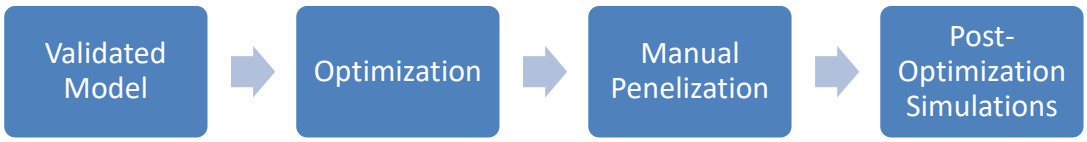


Figure 11 - Flowchart of the novel process

1- **Validated Model:** this includes obtaining a validated model, first obtaining the CAD of the part being optimized and other parts needed. This is to make the simple static simulation required were the loads of the optimizations are applied. After obtaining the model, validation for this model is required, this can be done by running the model and comparing it with other results from previous studies. **The output of this stage is a simple model static analysis.**

2- **Optimization:** After the model has been validated, comes the optimization stage. The first step before setting the constrains and other requirements of the optimization, a small modification is required in the CAD. This is to make the design area that will be selected for the optimization. This area is made by partitioning the part in ABAQUS. For this work because the design area is nonuniform, the inner part of the stem was separated and the stem skin was separated, then they were both combined into one part with the intersection boundaries between the two parts

remaining and then the stem was partitioned using these intersecting boundaries. After this, the optimization model is set starting from selecting the design area/region, then setting the objective function and the constrains required for the optimization and running the optimization once all is set. **The final output of this stage is one optimized femoral stem.**

3- **Manual Penalization:** the process as explained earlier is to produce as many stems as possible to fulfil accurate data plots for the key result being measured using the iso-surface value during the stem extraction process. This is basically when extracting the stems from ABAQUS optimization result tab, the required iso-surface value is used. For this work, 4 iso-surface values have been selected, 0.2,0.4,0.6 and 0.8. As there are two loads in this work, the walking load and the body weight load, and there are two materials, the total number of required optimization processes is four. **The result of this stage is 4 optimized stems from each optimization, thus total of 16 stems.**

4- **Post Optimization Simulations:** the aim of this stage is to simulate all the resultant stems for some required key results and plot the data with respect to the porosity/iso-surface value in order to find the optimum iso-surface/porosity value to suit the required later-on. As there are two loads in this work and 16 optimized stems, a total of 32 simulations were performed and the results were plotted as in the results section. Later on, when the optimum value is selected by medical researchers for further studies, the stem is extracted from the optimization files back from the output of stage 2 with the optimum iso-surface value.

The novelty of the process includes two parts, the first one is the manual penalization done after the optimization and the second part is the post-optimization

simulations. The purpose of the first part is to produce stems of different porosities using a threshold values as mentioned earlier. The second part is to evaluate and finding the trend in the performance, the process is extracting as many parts as possible with different porosities and simulating them recoding the key data used for selection of the required part. From the empirical equations of the fitting of the data of the key results, the exact required threshold will be found the part is extracted again using this threshold.

## 3.2. Finite Element Model

### *3.2.1. CAD*

The model used was obtained from previous studies were the femur bone and the stem used were obtained from a CT-Scan and imported into Abaqus (Alkhatib et al., 2019)(Jetté, Brailovski, Simoneau, Dumas, & Terriault, 2018). The femur bone was then cut from the bottom and inserted in a resin block for validation and boundary condition purposes (Jetté et al., 2018). The following parts were used in the assembly of the model:

1- The femur bone
2- The femoral stem
3- Epoxy Block
4- Three muscle forces application point pieces.

All of the parts are solid deformable parts.

5- 0 thickness part connected to stem head to apply force (Rigid, Planer) (Shown in the assembly figure only.

The following figures show the parts and the final assembly

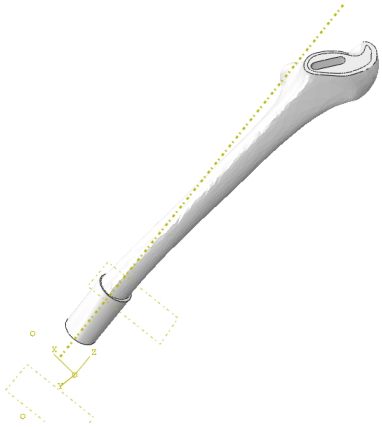

Figure 12 - Femur bone after cut

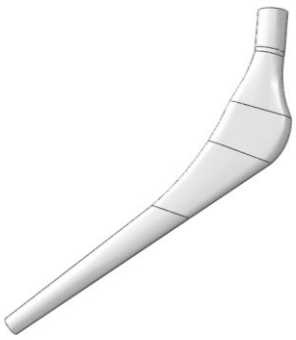

Figure 13 - Femoral Stem used

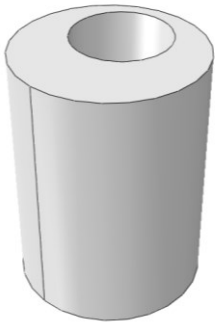

Figure 14 - Sample of muscle forces application points

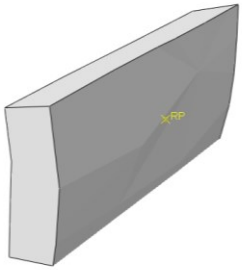


Figure 15 - Epoxy block to fix the stem


Figure 16 - The final assembly

### *3.2.2. Material Models*

Multiple material models were used as follows:

Bone material models: one for the cortical bone and one for the spongy bone. Both materials were assigned in ABAQUS material library as mentioned in the previous literature (Oshkour et al., 2015). The materials were then assigned as the following figure and the properties included elastic properties. The whole femur bone was set as Cortical Bone and the spongy part that is near the stem cut insertion point is spongy as in the figure.

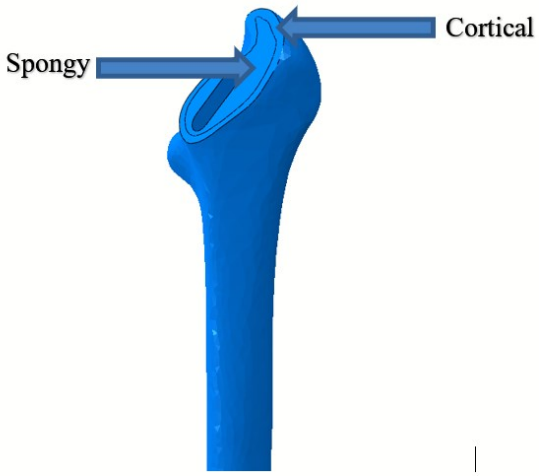


Figure 17 - Bone material assignment

The materials used for the stems were two materials, Ti-6Al-4V alloy (Arcam, 2014) (Aboutaleb, Mahtabi, Tschopp, & Bian, 2019) and -Co-Cr-Mo alloy (Lee, Nomura, & Chiba, 2008). The models for them were obtained from the literature and applied in ABAQUS data base and assigned to the stem body. Both material models included elastic and plastic properties can be found in the appendix. The plastic properties were obtained from experimentally obtained stress-strain curves.

Material used for the epoxy block were obtained from the reference used for the validation from experimental data and assigned to the block including elastic properties (Jetté et al., 2018).

### *3.2.3. Interactions*

The interactions module in ABAQUS is to align the relations between the parts and the definition of their relationship. The following interactions have set in the simulation:

1- Interaction between the inner part of the bone and the stem:

It was set as a contact interaction with a coefficient of friction of 0.4 (Oshkour et al.,

2015) (Alkhatib et al., 2019). There are some literature that use 0.3 for the coefficient (Nuño, Groppetti, & Senin, 2006) (Takumi et al., 2015) (Ataollahi Oshkour et al., 2014) (Ramos, Completo, Relvas, & Simões, 2012) (W. C. Chen, Lai, Cheng, & Chang, 2014), comparisons between the two values have been conducted through simulations and both values results were matching thus no difference was found between 0.3 and 0.4.

2- Interaction between the force application points (Muscles and stem head) and the femur bone and the stem respectively:

The interaction between the force application points and the main parts (stem and femur bone) was set to tie condition to not allow any relevant movement between the force point and the main part.

3- Between the bone and the epoxy block:

Tie condition was set here as well

4- Force application parts alone:

Their interaction was set to a rigid body, they are supposed to only transfer the forces to the main part.

### *3.2.4. Forces on the Hip Joint/loads*

The loads and boundary conditions are applied in two cases, walking loads and standing/body weight load. There is a common boundary as follows:

Fixed boundary condition to fix the epoxy block in-place:

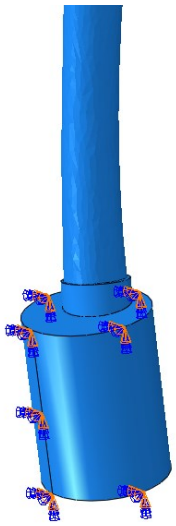

Figure 18 - Epoxy Boundary Condition

The not common forces depend on the case being simulated, as mentioned earlier, two cases are being studied, walking case and Body weight/standing case.

1- Walking loads:

The loads have been applied as in the same manner as the reference used for the walking loads as follows:

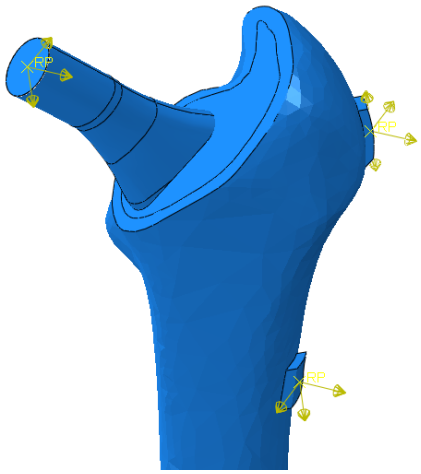

Figure 19 - Walking loads as per the reference

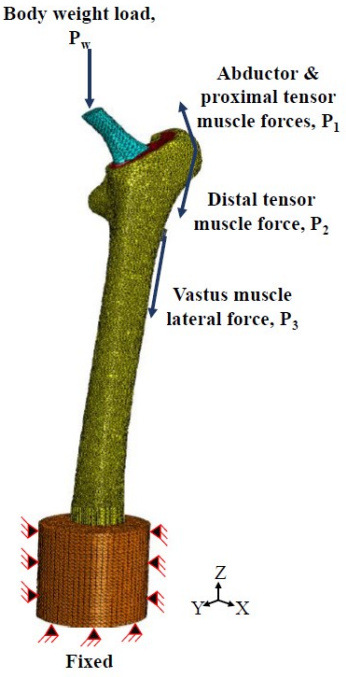


Figure 20 - Walking loads (Alkhatib et al., 2019)

The following table shows the assignment of the loads:

Table 1 - All Loads Used for Waling Load Simulations

| | **Load** | | |
|---|---|---|---|
| | **X (N)** | **Y (N)** | **Z (N)** |
| **$P_w$** | -378 | -229.6 | -1604.4 |
| **$P_1$** | 406 | 30.1 | 605.5 |
| **$P_1$** | 50.4 | 81.2 | 92.4 |
| **$P_2$** | -3.5 | -4.9 | -133 |
| **$P_3$** | -6.3 | 129.5 | -650.3 |

1- Body weight load:

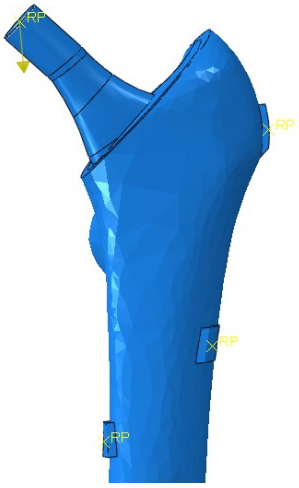


Figure 21 - Body weight load – yellow arrow on the stem head shows the direction

A simple load representing a 335% of body weight was applied at the stem head in the direction downwards representing the load applied for some daily routines in the case of standing for a body mass of 90.8 kg relative to the length of the femur being modelled (Jetté et al., 2018).

### *3.2.5. Validation*

The validation was done in comparison between what (Jetté et al., 2018) and the model we have, the validation was done for the body weight load as to compare with their experimental and numerical data. The following is the force vs displacement curve including the experimental data measured from their experiment and the numerical displacement measured from this model.

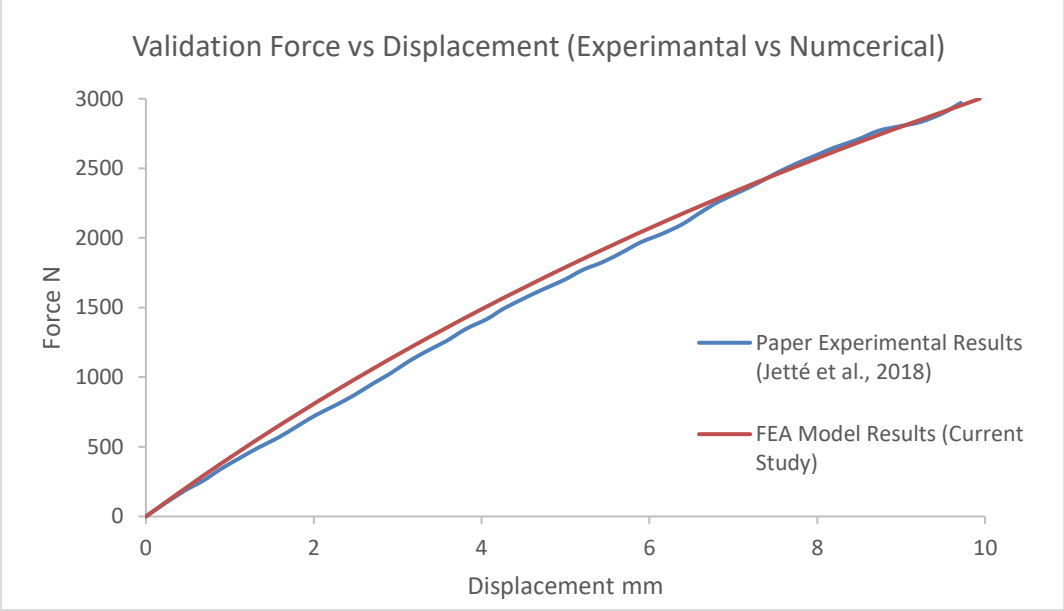


Figure 22 - Force vs Displacement Validation (Jetté et al., 2018)

It can be seen from the graph that the forces applied and the displacements caused with each the values of the force applied between the experimental done in the lab and the numerical values obtained from the model being used. Since the first match in and FE model is the displacement and force, it is more adequate to compare stress values for further matching but no data was found for the similar case conducted, the following shows the stresses in the femur bone from the same condition used for the validation.

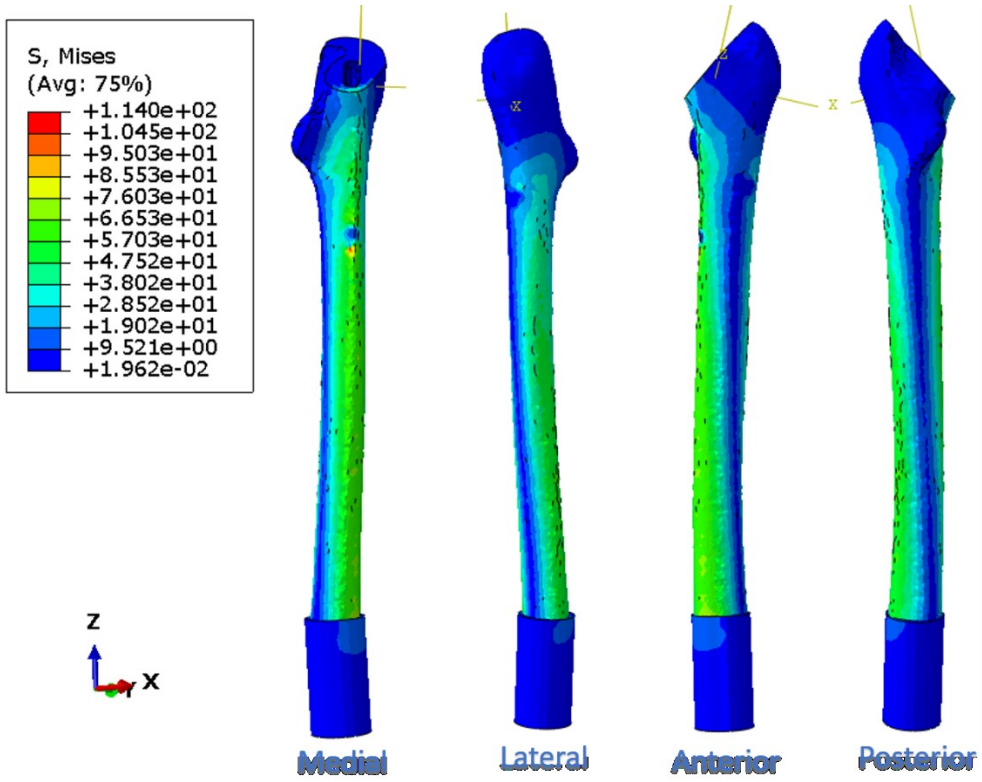


Figure 23 - Stresses in the femur bone - Validation Simulation

### *3.2.6. Meshing*

An element size of 1.8 for the stem has been used. Force application point as well used 1.8, where (Yamako et al., 2017) used 2 for a stem of the same length. In addition to 30 for the bone. Mesh information are as follows:

1- Femur: Tetrahedral elements, 17547 elements

2- Stem: Tetrahedral elements, 47437 elements.

3- Stem head: linear triangular elements, 42 elements.

Total Number or elements 65026 elements.

## 3.3. Optimization Model

### *3.3.1. CAD*

The same cad that was used in the static simulation was used except for the modification of the stem. The modification was to make a layer of approximately 1 mm of the material surrounding the design space (the part where the material will be removed during the optimization process). This is to get femoral stems optimized without compromising the shape and coatings being used in the off-shelf stems to use it directly with the same technique and tools to implant directly. The two parts were then assembled together as one part and the model was ready. This step was done to make it possible to select the inner region of the stem as a design space in the optimization process. The following figure shows the selection of the design space for the stem selected for the optimization process.

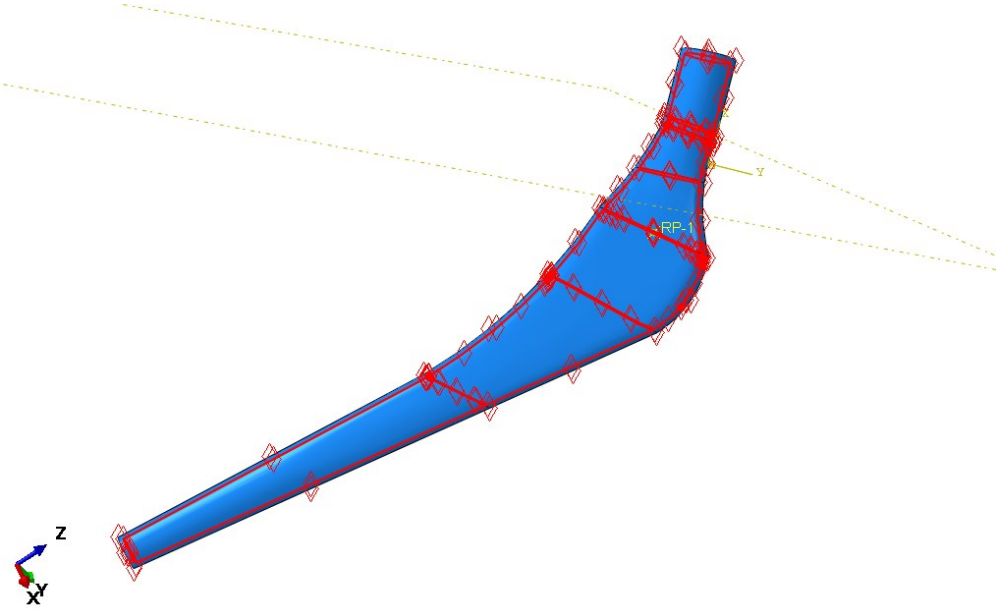


Figure 24 - Selected Design space for the optimization

### *3.3.2. Objective Function*

The objective function was to minimize the strain energy in the stem in order to increase the strain energy in the bone and thus the objective function was set to minimizing the strain energy in the stem as the increase of the strain energy in bone enhances the bone growth (Doblaré, García, & Gómez, 2004)(Energy, n.d.).

### *3.3.3. Constrains*

One constrains was used on the design region as follows:

- Volume constrain: a fraction of the initial value = 0.75.
- This is to reduce the volume of the inner region by 25% of the original value

## 3.4. Design of Experiment

The experiment objective is to illustrate a unique process of optimizing a femoral stem that can be printed using 3D metal printing/Additive Manufacturing solving the problem of relative density elements and having as many stems as possible for the data fitting without having to do optimization for each stem. To illustrate this, 4 optimization processes were done, and their results were converted into solid stems by using different thresholds and then the stems were tested using a static test. The process can be explained in two sections as follows:

### *3.4.1. Optimization of Stems*

The optimization process was done for two materials of the stem (Ti-6Al-4V and Co-Cr-Mo) and for two loads (Body Weight load and Walking loads). Resulting in 4 optimization processes that were carried out on the personal laptop with 8 cores clocking at 3.6 GHz and 16 GB of Ram combined with an SSD. Simulation times were approximately 40-50 hours per optimization process summarized to 187 hours in total for optimization only.

### *3.4.2. Simulation of Optimized Stems (Post Optimization)*

Four threshold values were selected, 0.2,0.4,0.6 and 0.8. These are the values that were used while converting the stems into solid. The result is 16 optimized femoral stems and two loads to test the performance with thus gathering into 32 femoral stems to be simulated. The following figure shows the tree of the simulations that were done:

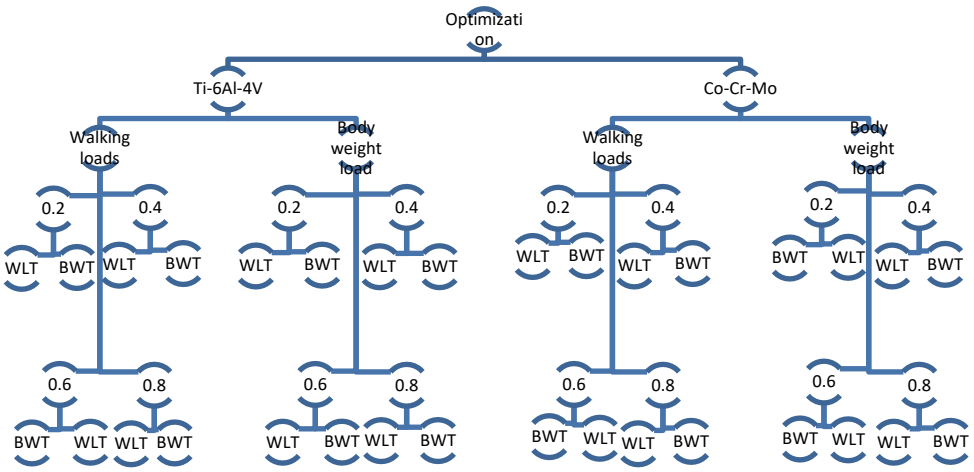


Figure 25 - Tree showing the optimization process inputs and the resulting outputs

# CHAPTER 4 : RESULTS AND DISCUSSION

## 4.1. The Optimized Stems

The following figures are showing a cross section of the resulting femoral stems from the optimization process, as mentioned earlier the exterior of the stems remains exactly the same as the solid and the difference is the inner region. There are four figures, two materials and two optimization loads are used and each figure contains the cross section of four stems for each of the four thresholds that were used for the conversion to printable stems.

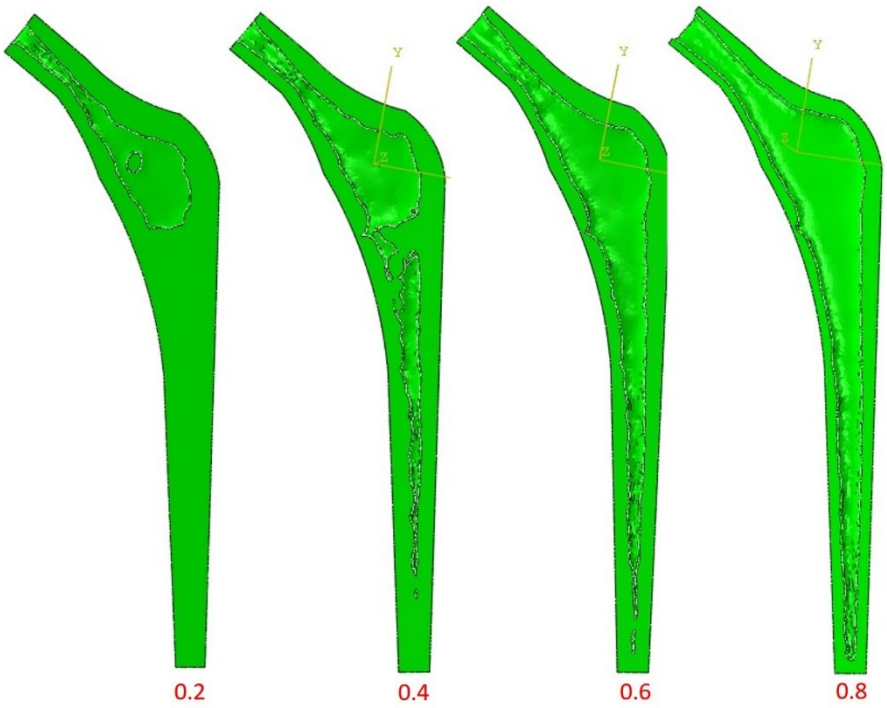


Figure 26 - Ti-6Al-4V optimized stems using body weight load

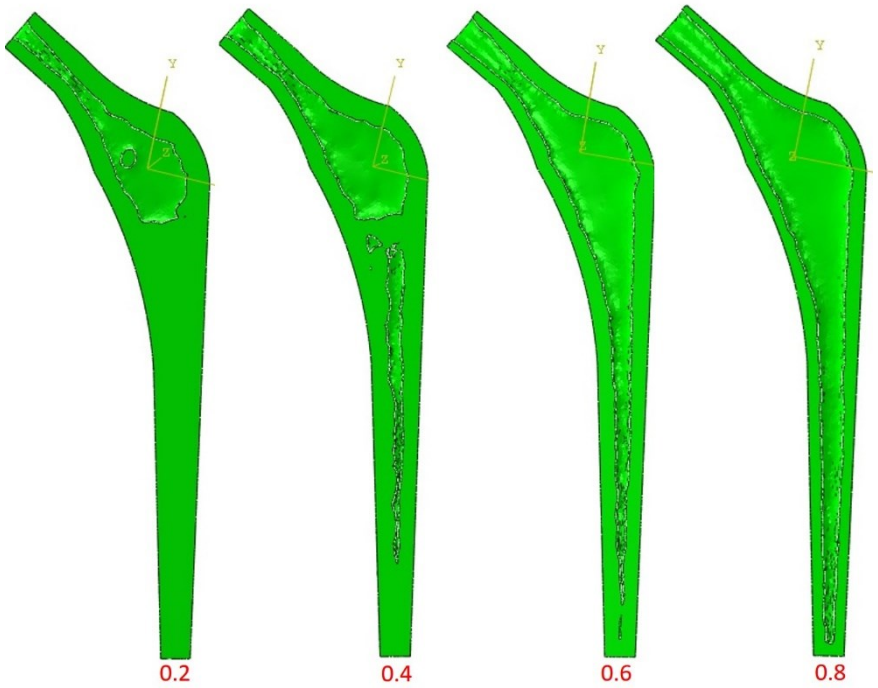


Figure 27 - Ti-6Al-4V optimized stems using walking loads

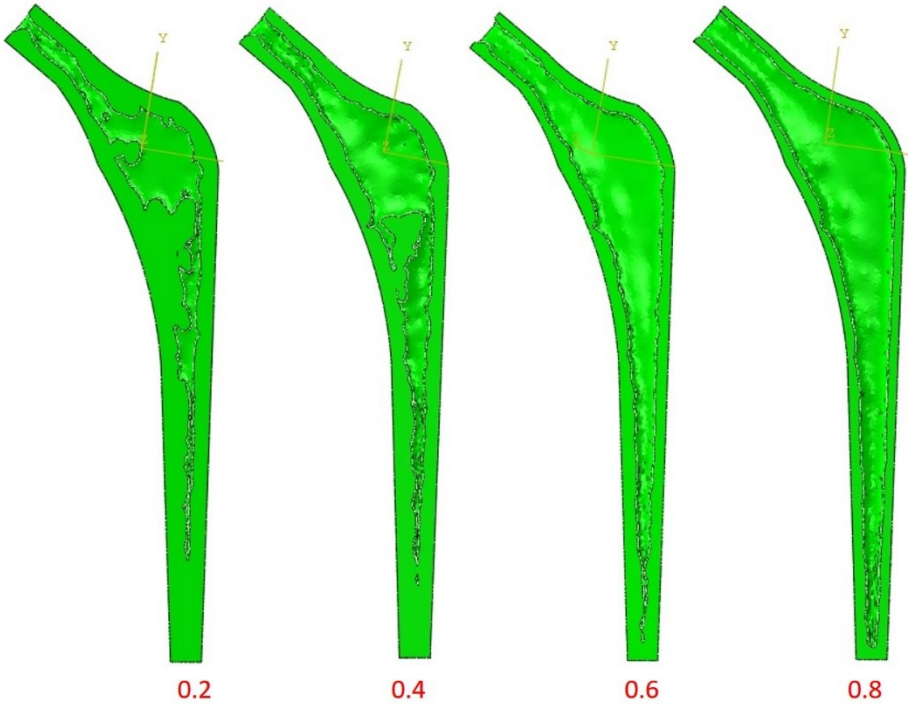


Figure 28 - Co-Cr-Mo optimized stems using body weight load

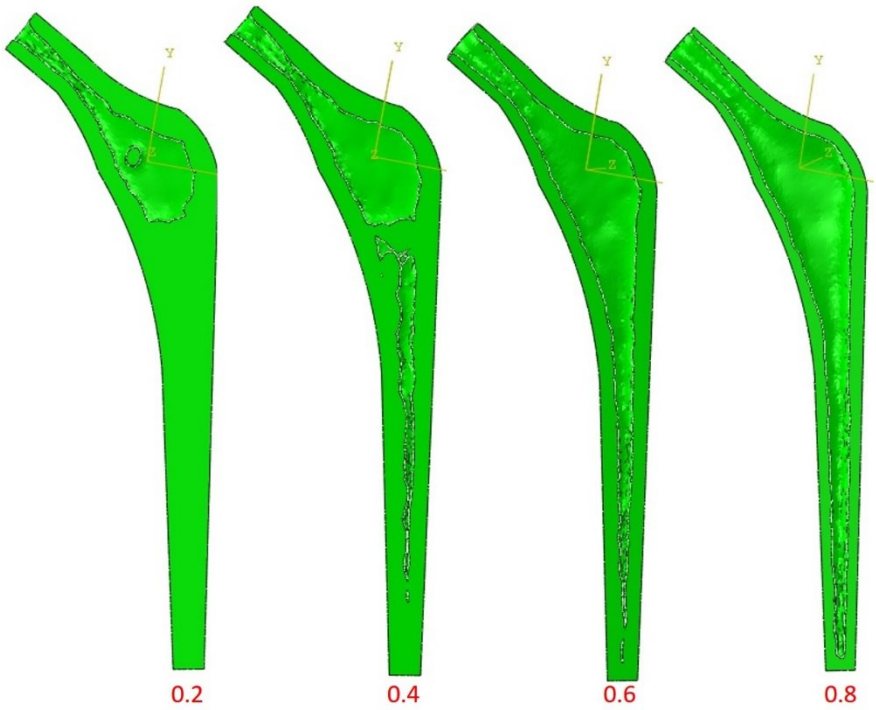


Figure 29 - Co-Cr-Mo optimized stems using walking loads

The observations to be noted here is the increase of the voids inside the stems with the increase of the threshold meaning less material in the extracted stem.

Other notices were the approximate similarities of the void shape with the load despite the change of the material.

In the figure showing the Co-Cr-Mo optimized using body weight load (Figure 27), the stem of 0.2 threshold has more voids than its counterparts, this is due to the cross-section level the screen capture was taken at was different than the other stems, not related to the actual void as proved by the porosity calculations shown in the next table.

The following table shows the calculated porosity of resulting stems in accordance to extraction threshold. The porosities were calculated using the material volume per optimized stem to the material volume of a solid stem:

Table 2 - Optimized Stems Porosities

| Thres hold | Ti Walking Load Test% | Ti Body Weight Test% | Co Walking Load Test% | Co Body Weight Test% |
|---|---|---|---|---|
| **0.2** | 5.15 | 5.06 | 5.23 | 6.12 |
| **0.4** | 10.98 | 11.07 | 10.99 | 13.81 |
| **0.6** | 22.40 | 22.72 | 22.62 | 27.30 |
| **0.8** | 34.57 | 34.85 | 34.56 | 39.87 |

Observations shows that the porosities across all stems and loads used for optimizing them are similar in values except for the Co-Cr-Mo stems optimized using the body weight load that have larger porosity. This is due to the greater stiffness of Co-Cr-Mo alloy compared to the other Ti alloy and of the body weight requires the stems to be stiffer and thus the material is arranged around the outer part of the stem creating more void.

### 4.2. Micromotions

The micromotions happening between the bone and the stem are of a great significance as they are the main factor in determining how the bone growth happens to stabilize the cement-less femoral stem. After the implantation is done, the bone tissue will take 4 to 12 weeks to form and the process will continue up to three years after the surgery, during this time a range of micromotions has be maintained in order to get the bone tissue suitable, the range is between 40 μm to 150 μm (Karuppal, 2016)(Limmahakhun et al., 2017). If any failure in providing the required range, it will lead either to loose implant if more motions occur, and too stiff implant if the opposite (Currey et al., 2013).

The micromotions were measured as the relevant motion between the stem and the femur bone and the dominant motion was found to be on the Y-axis direction as this is the load of the body weight is acting, even during the walking load condition.

The following sections show the micromotions for the optimized stems with reference to a solid stem with the same loads applied for each of the 4 cases that include: Ti-6Al-4V with body weight load, Ti-6Al-4V with the walking loads applied, Co-Cr-Mo with the body weight, and Co-Cr-Mo with the walking loads applied. The figures will include the optimized stems with the threshold starting from 0.2 on the left side to 0.8followed by the fully solid stem test of same material and loads as the last on the right. The legend on the left corresponds to the four optimized stems from the left and the legend on the right corresponds to the solid stem just besides it.

### *4.2.1. Ti-6Al-4V Optimized using walking loads*

1- Walking load simulation:

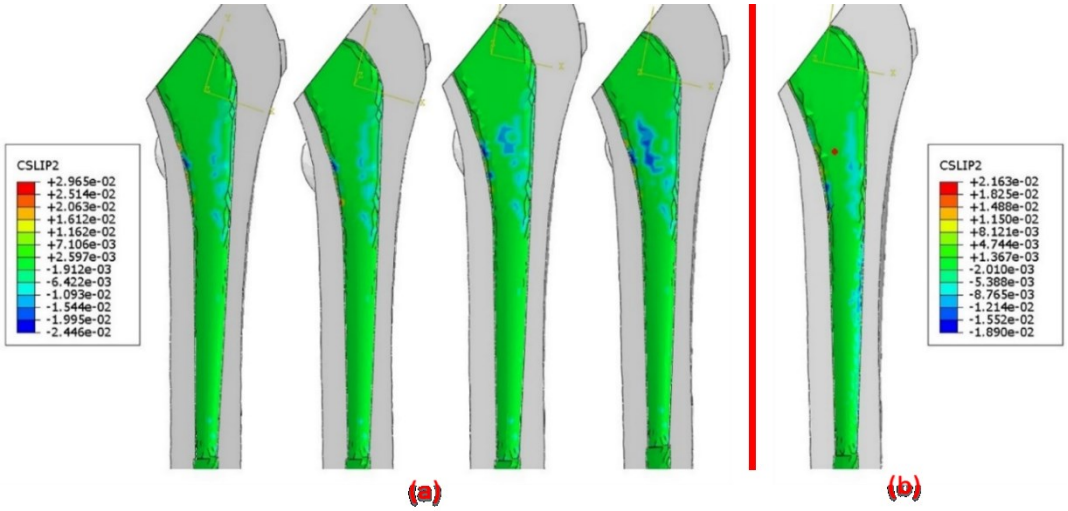


Figure 30 – (a) Titanium optimized stems optimized using walking loads - (b) Solid Stem – simulated under walking load condition

Observations of the figure indicate larger micromotions in the optimized stems were in the solid the range is between 1.3 and 21 μm, the range in the optimized stems is between 1.9 and 29 μm. The micromotions were observed to be increasing with the increase of the threshold (increased porosity) were is the optimized stem with 0.2 threshold has less micromotions than the one with 0.8. A second observation worth noting is the distribution of the micromotions as it is more uniform in the optimized stems than the solid stem. It is important to note that the micromotions observed in both optimized and solid stems here are below the requirement for proper bone ingrowth, this is mainly due to the over conservative coefficient of friction used for the simulation.

2- Body weight load simulation:

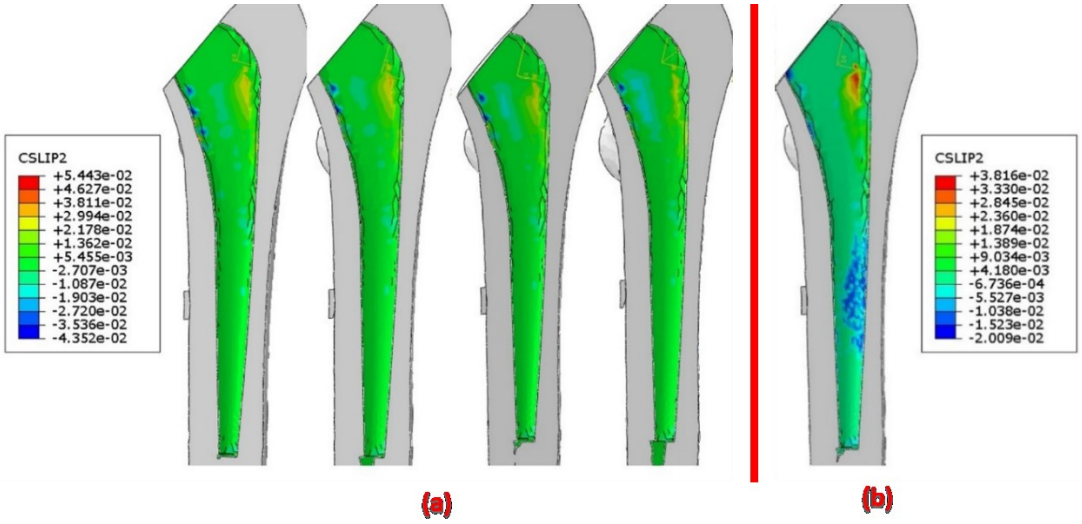


Figure 31 – (a) Titanium optimized stems optimized using walking loads - (b) Solid stem – simulated under body weight load condition

Observations here similar to the walking load in terms of the motion distributions, as they are more uniform in the optimized stems. The range of the motion in the body weight case covers larger gap as it ranges between 2.7 and 54 μm while the solid stem covers only 0.6 to 38 μm. The observation is also logical as the body weight load is more in magnitude in the direction where the dominant micromotions are being measured. The similar observation of increasing motion with increase of threshold is valid here as well.

### *4.2.2. Ti-6Al-4V Optimized using body weight loads*

1- Walking load simulation:

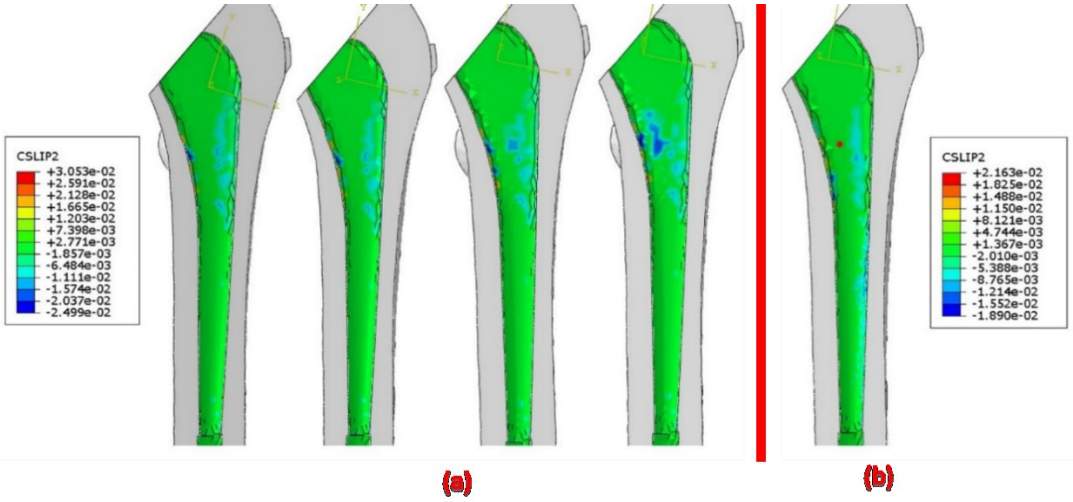


Figure 32 – (a) Titanium optimized stems using body weight load (b) Solid stems - simulated under walking load condition

The observations remain the same here except the larger range when compared with Figure 30 where the same load was applied as the motions in the optimized stems are slightly more in magnitude ranging from 1.8 to 30 μm. Other valid observations include the increase of motion with the increase of the threshold being extracted at.

2- Body weight load simulation:

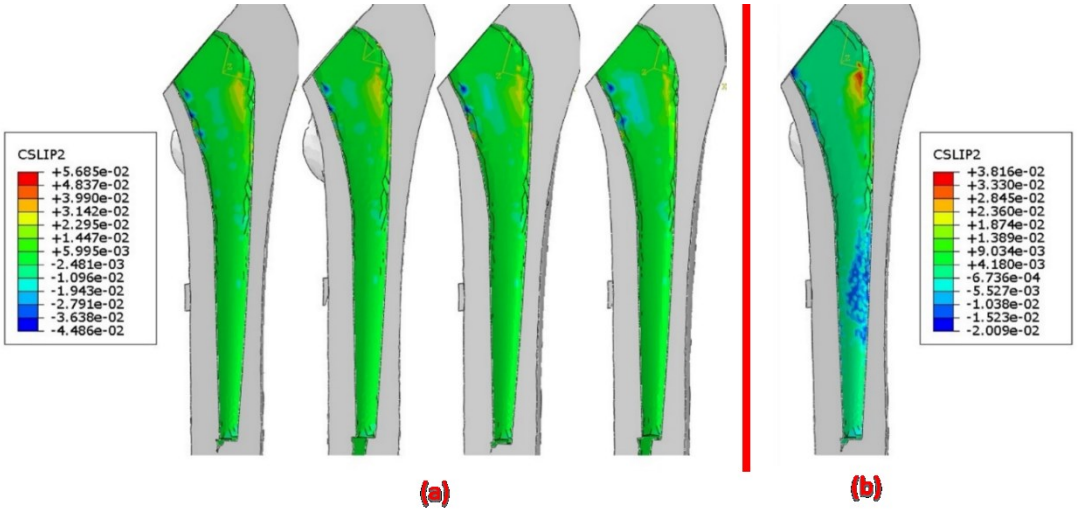


Figure 33 – (a) Titanium optimized stems using body weight load – (b) Solid stems - simulated under body weight load condition

Observations remain the same for the larger motions than the solid stem, increase of the motion with increase of the threshold and the uniformly distributed motion. Range witnessed is between 2.5 and 56 µm.

### *4.2.3. Co-Cr-Mo Optimized using walking loads*

1- Walking load simulation:

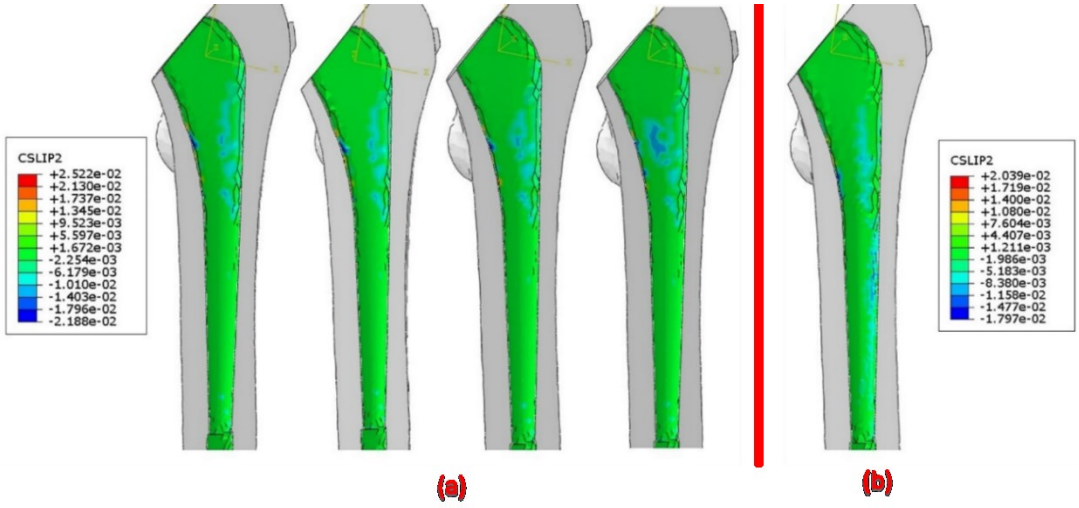


Figure 34 – (a) Co-Cr-Mo optimized stems using walking loads – (b) Solid stems - simulated under walking load condition

The observations remain the same with uniform distribution and increase with increasing threshold. The range difference however is more in the optimized stems than the solid, but the difference is not as large as the difference in the Ti-6Al-4V (Refer to the Figure/s of Ti here). This is due to the larger stiffness of Co-Cr-Mo alloy than Ti-6Al-4V. The range seen is between 1.6 and 25 μm.

2- Body weight load simulation:

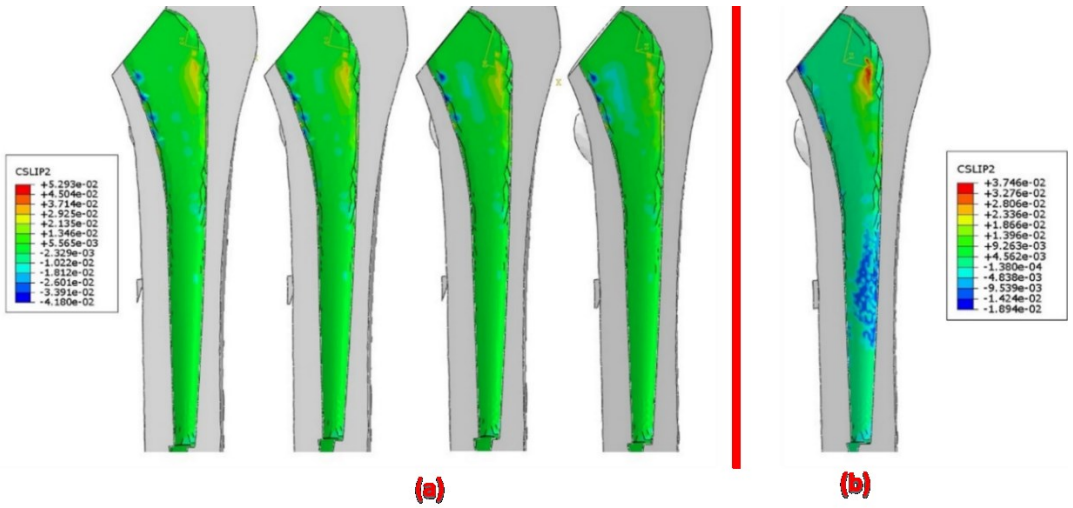


Figure 35 – (a) Co-Cr-Mo optimized stems using walking loads – (b) Solid stems - simulated under body weight load condition

Uniform distribution, larger range of motion between 2.4 and 53 micromotions are witnessed and the increase of motion with increase of threshold value is noticed. Less micromotion range again for the solid stem than the Ti-6Al-4V counterparts due to larger stiffness of Co-Cr-Mo.

### *4.2.4. Co-Cr-Mo Optimized using body weight loads*

1- Walking load simulation:

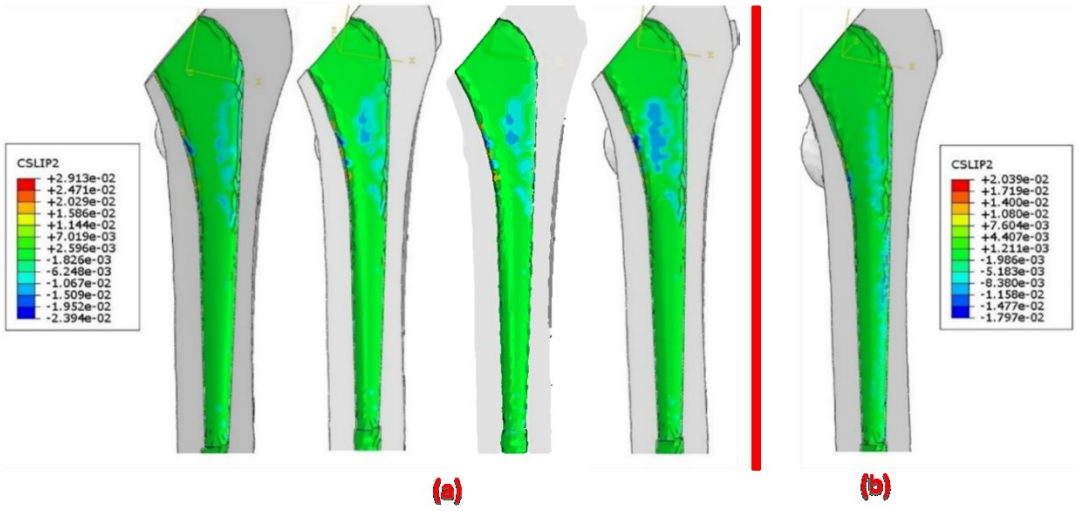


Figure 36 – (a) Co-Cr-Mo optimized stems using body weight load - (b) Solid Stem - simulated under walking load condition

Observations remain similar, the increase of motion with the increase of porosity. The range is larger as the remaining results of having range between 1.8 and 29 μm.

2- Body weight load simulation:

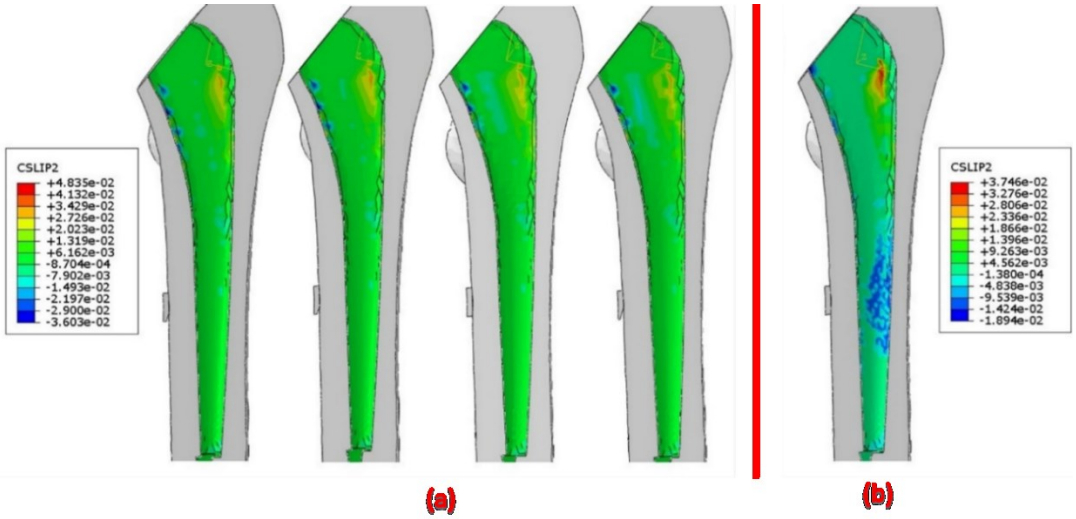


Figure 37 – (a) Co-Cr-Mo optimized stems using body weight load – (b) Solid Stems - simulated under body weight load condition

Observations remain the same as well, the uniform distribution, the increase with the threshold increase and the larger range between 0.8 and 48 µm.

### *4.2.5. Summary*

The range of micromotions between all the stems can be summarized as in the following tables, the first one for the stems optimized using the body weight load followed by a table for the stems optimized using the walking load:

Table 3 - Micromotions Range for The Stems Optimized Using the Body Weight Load

| | **Ti-6Al-4V** | | **Co-Cr-Mo** | |
|---|---|---|---|---|
| **Threshold** | **Body Weight** | **Walking Load** | **Body Weight** | **Walking Load** |
| | **Test µm** | **Test µm** | **Test µm** | **Test µm** |
| **0.2** | 1.35 – 50.1 | 1.96 – 26.8 | 0.87 – 48.3 | 1.70 – 26.0 |
| **0.4** | 1.70 – 50.1 | 2.04 – 26.9 | 1.34 – 48.2 | 0.68 – 25.4 |
| **0.6** | 2.22 – 52.6 | 1.95 – 28.4 | 1.61 – 49.9 | 1.95 – 26.9 |
| **0.8** | 2.48 – 56.9 | 1.85 – 30.1 | 2.03 – 54.9 | 1.82 – 29.1 |
| **Solid** | 0.06 – 38.2 | 2.01 – 21.2 | 0.01 – 37.5 | 1.98 – 20.0 |

Table 4 - Micromotions Range for The Stems Optimized Using the Walking Load

| | Ti-6Al-4V | | Co-Cr-Mo | |
|---|---|---|---|---|
| **Threshold** | **Body Weight Test µm** | **Walking Load Test µm** | **Body Weight Test µm** | **Walking Load Test µm** |
| **0.2** | 1.34 – 50.0 | 1.96 – 26.8 | 0.98 – 48.6 | 1.67 – 25.0 |
| **0.4** | 1.48 – 50.0 | 1.99 – 26.7 | 1.13 – 48.6 | 1.72 – 25.1 |
| **0.6** | 2.09 – 51.6 | 2.02 – 28.0 | 1.78 – 50.0 | 2.01 – 26.3 |
| **0.8** | 2.71 – 54.4 | 1.91 – 29.6 | 2.32 – 52.3 | 2.03 – 27.9 |
| **Solid** | 0.06 – 38.2 | 2.01 – 21.2 | 0.01 – 37.5 | 1.98 – 20.0 |

The observations when comparing each of the stems for the same conditions and the same load and comparing them with the solid stems are as follows:

* The Ti-6Al-4V stems result in more micromotions within the required range which is better for bone growth within the pores than the Co-Cr-Mo counterpart (Limmahakhun et al., 2017). This indicates that the desired range of micromotions can be achieved independently of the material used.

* The solid stems result in less micromotions than the optimized stems indicating a bad bone growth (Limmahakhun et al., 2017).

* The micromotions are higher when the body weight load is applied as compared to the walking loads, as the magnitude of the body weight load is higher in the measurement direction.

* The micromotions increase as well with the increase of the threshold (meaning less void in the stem).

* The ranges witnessed in the results some of them are less than the required

range of motion for the bone growth that was the result of using an overestimation of the coefficient of friction.

### 4.3. Strain Energy in Spongy Bone

In this section, the relation between the strain energy and the porosity (void sizes percentage) is addressed. The following four figures show the relation where the strain energy increase in percentage is on the Y-axis and the porosity percentage is on the X-axis. There are four subsections categorized by the material and the load applied for the post-optimization simulation.

#### *4.3.1. Ti-6Al-4V stems simulated under Body weight load*

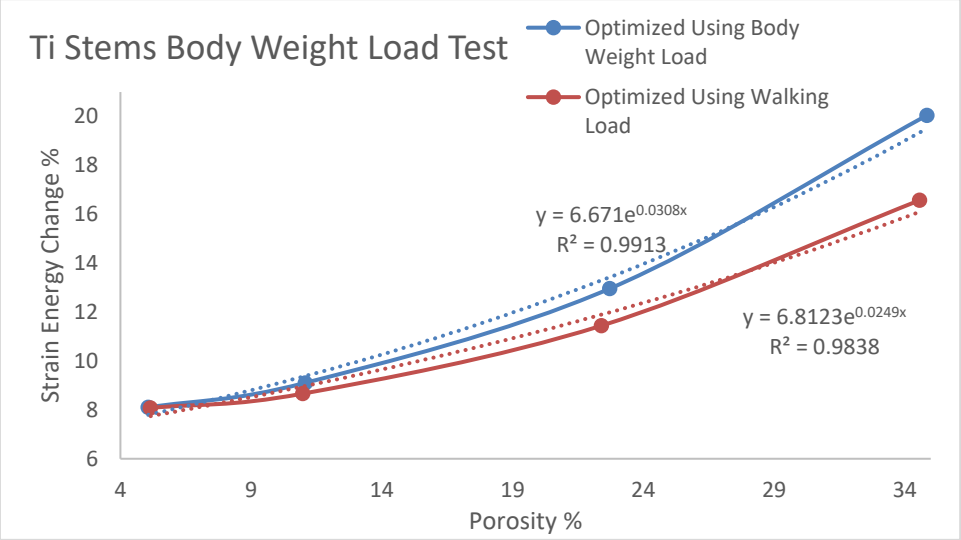


Figure 38 - Strain energy increase in femur bone under body weight load

The observations seen include the following from the graph:

* The larger increase in the strain energy in the bone when the stem is optimized using the body weight load rather than the stems optimized using the walking load. This is due to the larger load applied during the optimization in the body

weight optimized stems than the walking load.

* The increase of the strain energy increase in the bone with the increase of porosity of the stems. This is due to the stems becoming less stiff transferring more strain energy to the bone than the more solid stems that are of less porosity (Oshkour et al., 2015).

### *4.3.2. Ti-6Al-4V stems simulated under Waling loads*

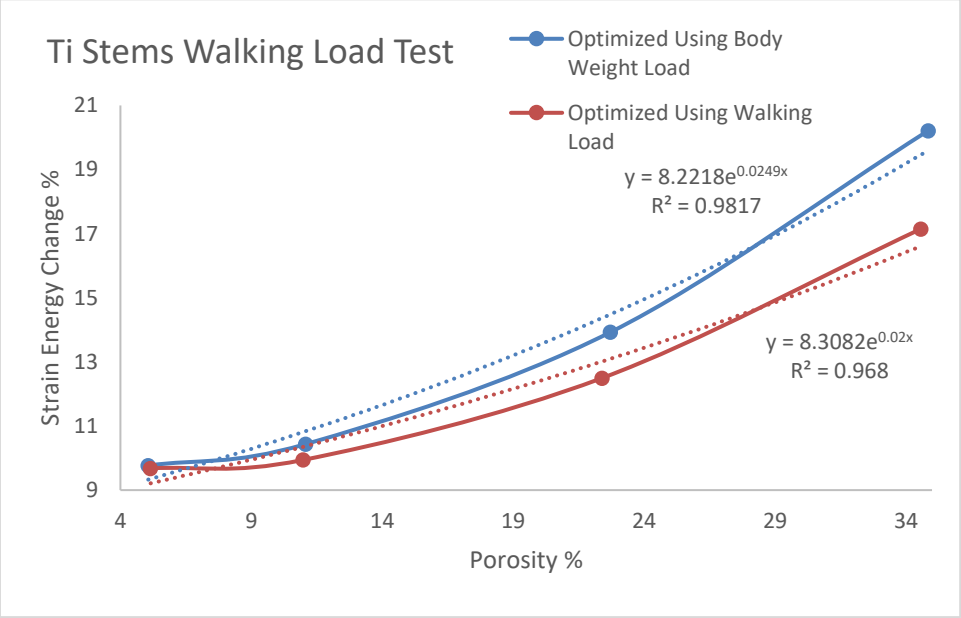


Figure 39 - Strain energy increase percentage vs Stem Porosity – Ti-6Al-4V under walking load

The observations of this result are as follows:

* The increase of strain energy change in the bone for the stems optimized using the body weight load over the stem optimized using the all load conditions. This is due to the larger load applied during the optimization in the body weight optimized stems than the walking load.

* The increase of the strain energy change in the bone with the increase of the porosity of the stems, this is due to the stems becoming less stiff when they have larger porosities than the solids stems transferring more load to the bone as the energy is reduced in the stems and increased in the bone.

### *4.3.3. Co-Cr-Mo stems simulated under body weight load*

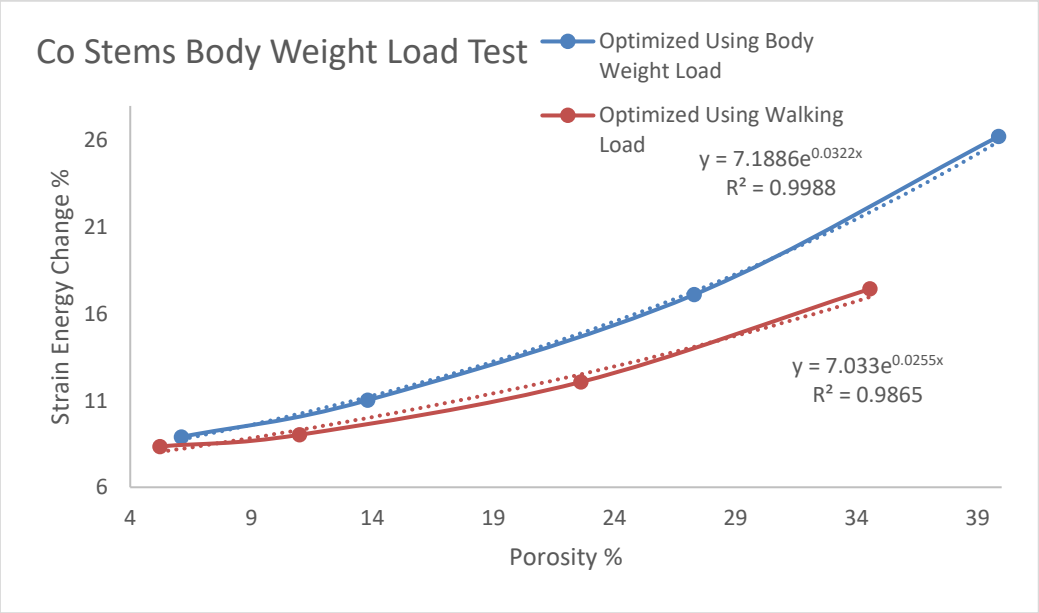


Figure 40 - Strain energy increase percentage vs Stem Porosity – Co-Cr-Mo under body weight load

The observations are the same as the two previous results, that for stems optimized using body weight in the Ti-6Al-4V stems have a strain energy increase of up to 20% while for the Co-Cr-Mo counterparts the increase is up to 25% and for the stems optimized using the walking load Ti-6Al-4V the increase was not as clear as in the previous case this is due to the higher porosity achieved in the Co-Cr-Mo stems optimized using the body weight load as the max porosity for them was 39% and for

the Ti-6Al-4V counterparts was only 34% and for Co-Cr-Mo stems optimized using the walking load as well the most porous stem had 34%, this is due to the larger load applied in the optimization for the body weight load optimized Co-Cr-Mo stems and the larger stiffness compared to the Ti-6Al-4V stems optimized under body weight.

### *4.3.4. Co-Cr-Mo stems simulated under walking loads*

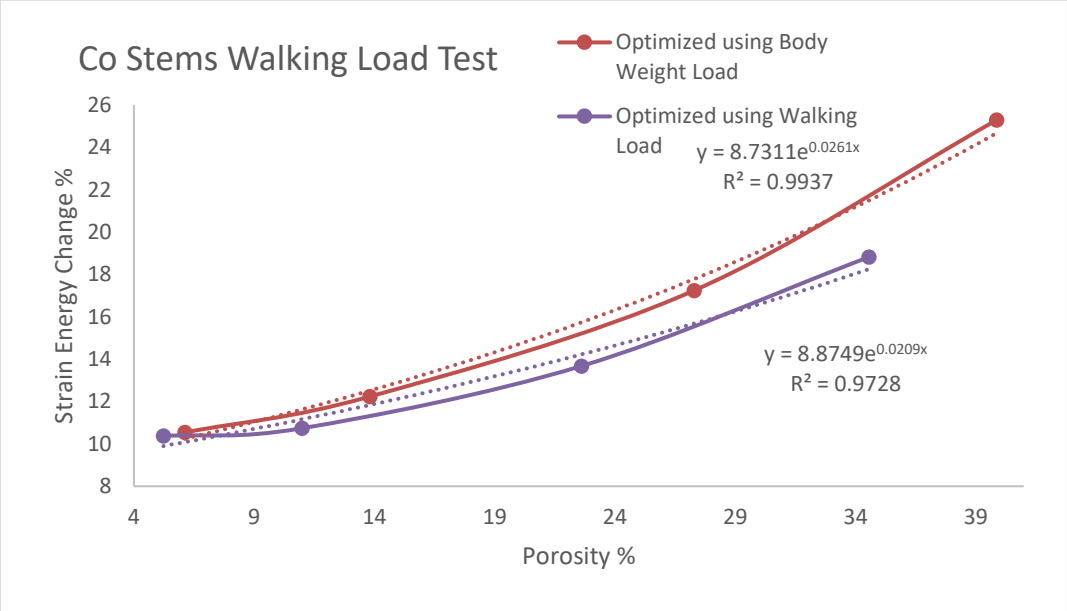


Figure 41 - Strain energy increase percentage vs Stem Porosity – Co-Cr-Mo under walking load

Observations here are similar to the previous sections and include:

* The increase of strain energy change in the bone for the stems optimized using the body weight load than the stems optimized using the walking loads. This is due to the larger load applied during the optimization in the body weight optimized stems than the walking load.

* The increase of strain energy change in the bone with the increase of porosity

of the stem. This is due to the stems becoming less stiff making it have less strain energy allowing this strain energy to be transferred to the bone.

### *4.3.5. Summary*

The change in the strain energy in the bone is seen to be directly proportional to the change in the porosity of the stems for all of the cases. The main observation was the greater amount of change in strain energy in the stems optimized using the body weight load relative to the stems optimized using the walking loads for both materials. This is due to the larger load applied during the optimization process in the case of optimizing the stems using the body weight load. In addition to the noticeable increase of strain energy change in the bone with the change in porosity for all stems under the same load and optimized using the same conditions. The relation between the porosity of stems and the strain energy increase in bone is due to the stems becoming less stiff allowing more strain energy transfer to the bone. The following table summarises the percentage change in strain energy with respect to the porosity for all cases addressed above.

1- Stems optimized using body weight load:

Table 5 - Strain Energy Change in The Bone for Stems Optimized Using Body Weight Load

| | | Ti-6Al-4V | | | Co-Cr-Mo | |
|---|---|---|---|---|---|---|
| **Threshold** | **Porosity %** | **Body Weight Strain Energy Increase %** | **Walking Load Strain Energy Increase %** | **Porosity %** | **Body Weight Strain Energy Increase %** | **Walking Load Strain Energy Increase %** |
| **0.2** | **5.06** | 8.10 | 9.77 | **5.11** | 9.98 | 10.53 |
| **0.4** | **11.07** | 9.11 | 10.44 | **10.53** | 11.44 | 12.24 |
| **0.6** | **22.72** | 12.96 | 13.93 | **22.85** | 15.69 | 17.24 |
| **0.8** | **34.85** | 20.05 | 20.21 | **34.65** | 21.57 | 25.29 |

2- Stems optimized using walking load:

Table 6 - Strain Energy Change in The Bone for Stems Optimized Using Walking Load

| | | Ti-6Al-4V | | | Co-Cr-Mo | |
|---|---|---|---|---|---|---|
| **Threshold** | **Porosity %** | **Body Weight Test Strain Energy Increase %** | **Walking Load Test Strain Energy Increase %** | **Porosity %** | **Body Weight Test Strain Energy Increase %** | **Walking Load Test Strain Energy Increase %** |
| **0.2** | **5.15** | 8.08 | 9.68 | **5.23** | 8.36 | 10.37 |
| **0.4** | **10.98** | 8.66 | 9.94 | **10.99** | 9.03 | 10.74 |
| **0.6** | **22.40** | 11.44 | 12.50 | **22.62** | 12.08 | 13.68 |
| **0.8** | **34.57** | 16.57 | 17.15 | **34.56** | 17.45 | 18.82 |

The strain energy change in bone is witnessed to have a constant increase regardless of the load being used in the post-optimization simulation. The constant increase however is related to the load used for the optimization of the stem. This includes the Ti-6Al-4V stems having a strain energy increase of 20% for the ones optimized using the body weight load and 17% for the ones optimized using the walking loads. For the Co-Cr-Mo counter parts, the strain energy for the ones optimized using the body weight was around 20% and for the ones optimized using

the walking load the strain energy is around 17%. All of these stems in this comparison had a porosity of around 34%.

In addition to that, the change of the strain energy in the bone is witnessed to have a directly proportional relationship with the porosity of the stems (that is directly dependent on the threshold being used). This means in order to get more strain energy increase in the bone, it is required to increase the porosity/void by increasing the threshold used for extracting the stems and this must be done without tolerating the factor of safety.

## 4.4. Extrapolation of Porosities and Results

### *4.4.1. Factor of safety calculations*

The objective of this section to show a prediction of the maximum achievable porosities in order to get the maximum achievable strain energy transfer to the bone. the following are the relation between the calculated factor of safety and the porosity in all of the stems. There are two figures gathered by the load applied in the post-optimization simulation as the stress results are ranging close together.

1- Walking load simulation

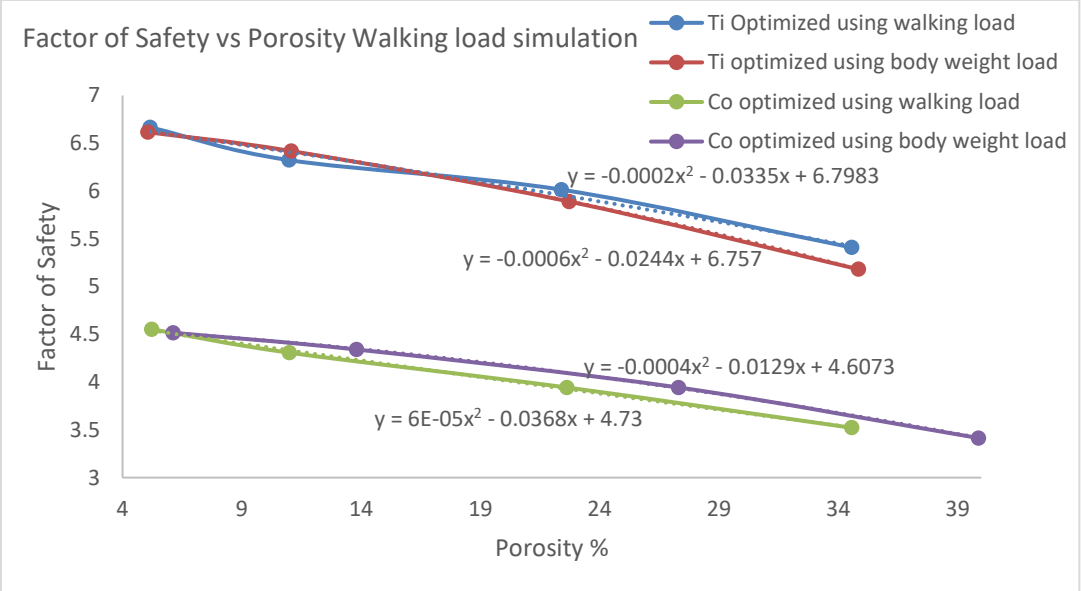


Figure 42 - Factor of Safety vs Porosity Walking load simulation

2- Body weight load simulation

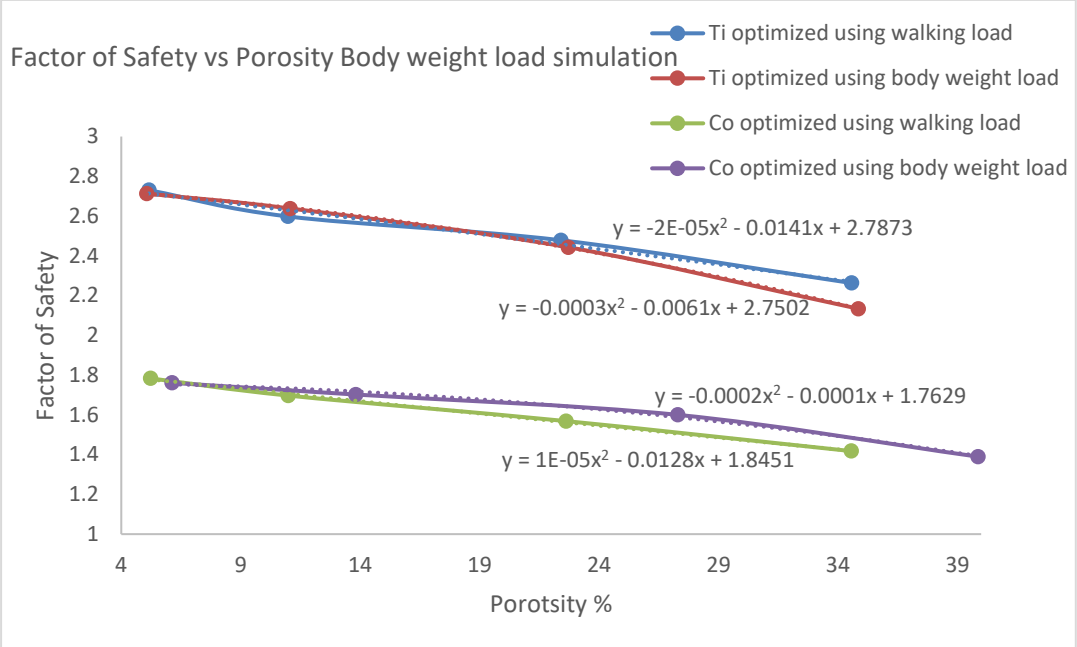


Figure 43 - Factor of Safety vs Porosity body weight load simulation

Observations to note in the previous figures indicate the higher factor of safety of Ti-6Al-4V alloy optimized stems rather than its Co-Cr-Mo counterparts. In addition to the expected lower factor of safety range for all stems when using the body weight load is used for the post-optimization simulation. The observed larger factor of safety for the Ti-6Al-4V stems is due to the larger yielding stress of the Ti-6Al-4V alloy than the Co-Cr-Mo. The stresses measured as well show a difference but it is not the main controlling fact controlling the factor of safety as the difference is not that large when comparing stems of the same porosity made from the two different materials. The following figures show the stresses with the porosity for both the waling load post-optimization simulations and the body weight simulations as well. The point where the stress was taken is the point of maximum stress which was the same for all

conditions, stems and loads, the point is shown in the next figure as follows in the red region circled by a black circle:

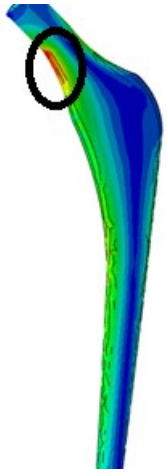

Figure 44 - Maximum Stress Point in stems

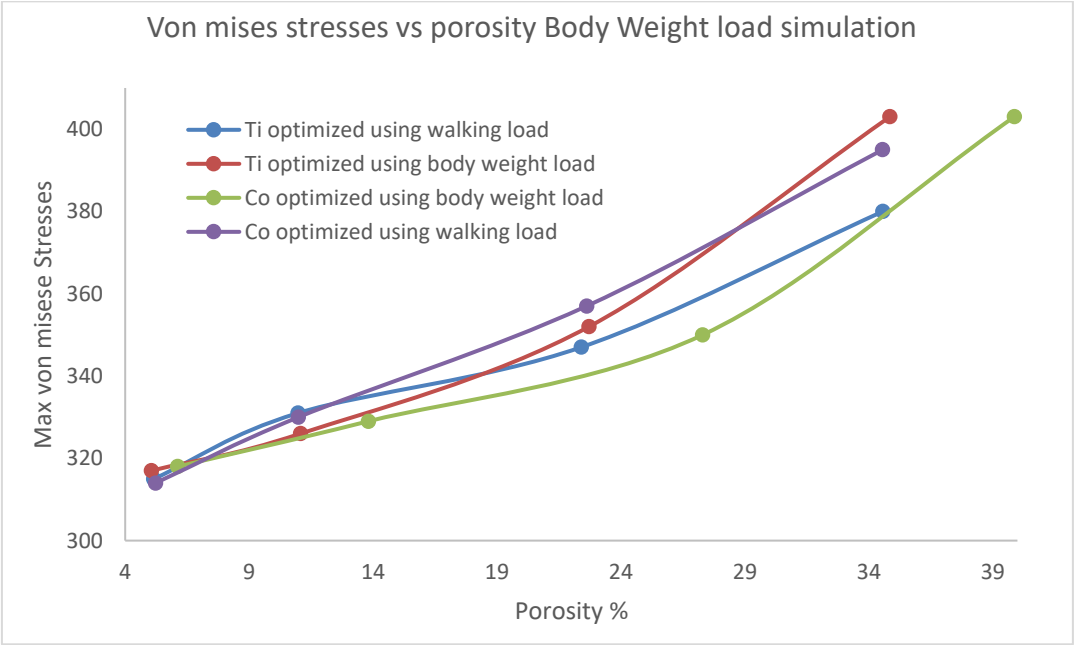


Figure 45 - Stresses vs the porosity for body weight load post-optimization simulation

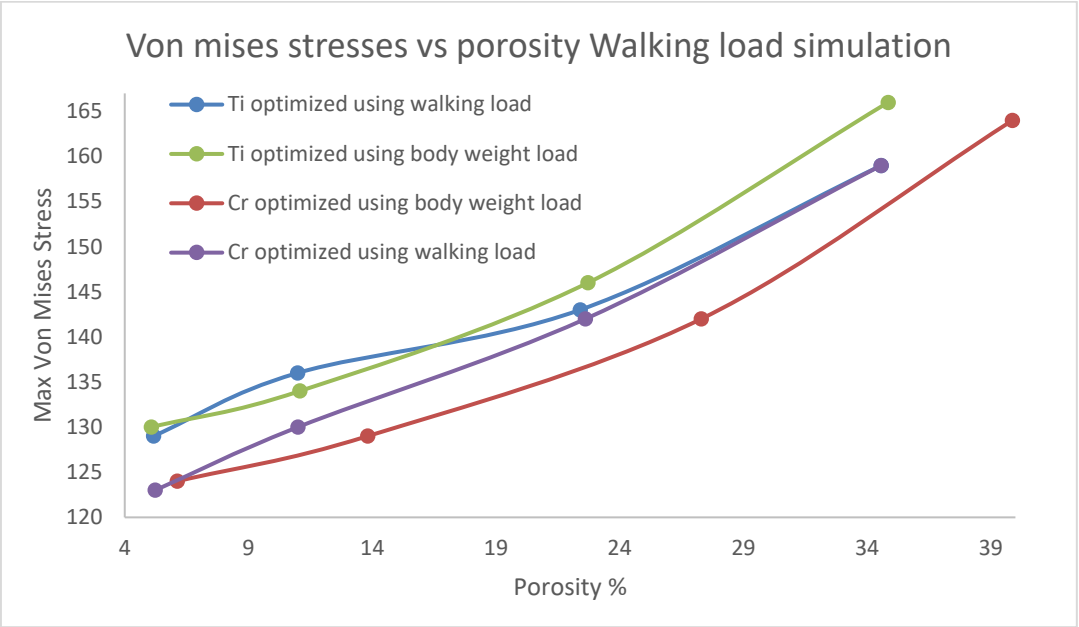


Figure 46 - Stresses vs the porosity for walking load post-optimization simulation

The predictions will be done on the walking load as it is not as exaggerated as the used body weight load and most of the available literature use the walking loads (Baharuddin et al., 2014)(Ebramzadeh, Sangiorgio, Longjohn, Buhari, & Dorr, 2004)(A Harris et al., 2014)(Chalernpon, Aroonjarattham, & Aroonjarattham, 2015). The following table shows the calculated factors of safety from the previous figures:

1- Ti-6Al-4V:

Table 7 - Ti-6Al-4V Stems Factors of Safety

| **Porosity %** | **Ti BW BWT** | **Ti BW WLT** | **Porosity %** | **Ti WL BWT** | **Ti WL WLT** |
|---|---|---|---|---|---|
| **5.06** | 2.71 | 6.62 | **5.15** | 2.73 | 6.66 |
| **11.07** | 2.64 | 6.42 | **10.98** | 2.60 | 6.32 |
| **22.72** | 2.44 | 5.89 | **22.40** | 2.48 | 6.01 |

| | | | | | |
|---|---|---|---|---|---|
| **34.85** | 2.13 | 5.18 | **34.57** | 2.26 | 5.40 |

2- Co-Cr-Mo:

Table 8 - Co-Cr-Mo Stems Factors of Safety

| **Porosity %** | **Co BW BWT** | **Co BW WLT** | **Porosity %** | **Co WL BWT** | **Co WL WLT** |
|---|---|---|---|---|---|
| **6.12** | 1.76 | 4.52 | **5.23** | 1.78 | 4.55 |
| **13.81** | 1.70 | 4.34 | **10.99** | 1.70 | 4.31 |
| **27.30** | 1.6 | 3.94 | **22.62** | 1.57 | 3.94 |
| **39.87** | 1.39 | 3.41 | **34.56** | 1.42 | 3.52 |

### *4.4.2. Extrapolations:*

The fit used in the graphs in the previous section are done using a polynomial equation of the second degree as an initial indication. Using a minimum factor of safety of 2.5 will be taken as a reference that the lowest to achieve using the extrapolations (A Harris et al., 2014). The calculated maximum achievable porosities for the stems under the walking load test can be found in the next table. These values were calculated using the fitting equations from the curves for the walking loads as mentioned earlier.

Table 9 - Maximum Achievable Porosities For Walking Load Conditions For A Factor Of Safety Of 2.5

| Stem | Max Porosity % | Max Strain energy Increase % |
|---|---|---|
| **Ti WL WLT** | 85.10 | 45.56% |
| **Ti BW WLT** | 66.30 | 42.85% |
| **Co WL WLT** | 68.20 | 36.91% |
| **Co BW WLT** | 58.20 | 39.88% |

The observation is that the maximum strain energy increase can be achieved using the Ti-6Al-4V stems over the Co-Cr-Mo due to the higher maximum achievable porosities. The values of the maximum strain energy increase were calculated using the curve fit equations used to the strain energy curves for the walking load test for both materials were the fit was done using an exponential equation.

The main requirement for the achievement of these porosities in design is computational power as will be discussed in the next chapter of conclusion and future work. These stems have to be designed and then tested as in the same process used here.

### 4.5. Printability of the Optimized stems

To test the printability of the stems optimized here as the main objective, Magics Materialise software has been used as it is the one used for conversion of the stems into solid parts as well and it has been used in the literature for the same purpose (Li, Wang, Zhang, & Li, 2009)(Brailovski, Jetté, Simoneau, Dumas, & Terriault, 2017)(K. Hazlehurst et al., 2013)(K. B. Hazlehurst, 2014)(Harrysson, Cansizoglu, Marcellin-Little, Cormier, & West, 2008)(Taniguchi et al., 2016). This software is being used to

convert the STL files of the optimized stems into slices where the printer can print them and prepare the support generation for the parts as well. The stems were successfully sliced, and their supports were done successfully with no issues and it is ready to print. Unfortunately, the part could not be printed due to failure in the machine thus no pictures of the printed part are shown.

# CHAPTER 5 : CONCLUSION AND FUTURE WORK

## 5.1. Conclusion

The aim of this work was to implement a novel process of optimizing femoral stems that can be printed using additive manufacturing machines/3D metal printing. The novelty in the work is the ability to print the optimized stems as the results of any optimization process are a map of the material density distribution containing elements of relative density that cannot be printed and to have more stems to simulate without paying the computational cost of having one optimization for each stem produced in order to have a customized optimized stems suiting the exact needed key requirements that are in this work chose to be the strain energy increase and the factor of safety. To illustrate the process, 16 femoral stems were designed using the optimization process using four optimization processes and the conversion process resulted in 16 optimized stems that had to be evaluated for their performance by applying two loads in a simulation process summing up to 32 post optimization simulations. Two materials were used that are commonly used alloys for the same implant in the current market, Ti-6Al-4V and Co-Cr-Mo. In addition to the two loads that were used, a walking load and a body weight load where the later simulates the standing of the patient.

The evaluation of the optimized stems was based on two main results, the micromotions in the bone tissue and the strain energy increase in the bone tissue. It was found out that the strain energy increase is related to the load used in the optimization process as the values of strain energy increase were the same and the stems optimized using the body weight load had more strain energy increase in the bone than the stems optimized using the walking load. This is due to the larger load used during the optimization using the body weight load.

For the micromotion evaluation, Ti-6Al-4V stems resulted in more micromotions within the range required to motivate bone growth than the Co-Cr-Mo counterparts by a slight increase of 1-2 μm. This slight difference shows that the range of motions desired can be achieved independent of the material.

A third evaluation was done to predict the maximum achievable strain energy increase in the bone by predicting the maximum achievable porosities. It was found that the maximum of increase in the Ti-6Al-4V stems is more than the Co-Cr-Mo stems.

To summarize, the use of Ti-6Al-4V for optimized stems is preferable for its slight better performance over Co-Cr-Mo in the more strain energy increase achievable and the larger micromotions range.

**5.2. Future Work**

The difficulties faced during the work were related to the computational power limits. This resulted in limiting the maximum used volume reduction constrain for the optimization process due to the limited mesh size used for the process. Thus, it is recommended in to use more powerful computers to use more volume reduction the in the optimization process to achieve more strain energy absorption in the bone. Other future work may include using a thinner skin size for the stem and this can be achieved again using more elements and a smaller mesh size. In addition to having more computational power will allow more optimization processes to be done allowing the studying of more factors like the material penalization relative density threshold as this requires a whole optimization process for each stem and one optimization process costs 50 hours of running.

# REFERENCES

A Harris, A. R., Baharuddin, M. Y., Noor, A. M., Majid, N. A., Abd Kader, A. S., Lee, M. H., … Salleh, S.-H. (2014). Design process of cementless femoral stem using a nonlinear three dimensional finite element analysis. *BMC Musculoskeletal Disorders*, *15*(1), 1–17. https://doi.org/10.1186/1471-2474-15-30

Aboutaleb, A. M., Mahtabi, M. J., Tschopp, M. A., & Bian, L. (2019). Multi-objective accelerated process optimization of mechanical properties in laser-based additive manufacturing: Case study on Selective Laser Melting (SLM) Ti-6Al-4V. *Journal of Manufacturing Processes*, *38*(January 2018), 432–444. https://doi.org/10.1016/j.jmapro.2018.12.040

Alkhatib, S., Tarlochan, F., Mehboob, H., Singh, R., Kadirgama, K., & Harun, W. S. W. (2019). *Finite element study of functionally graded porous femoral stems incorporating body centered cubic structure*. *Artificial Organs*. https://doi.org/10.1111/aor.13444

Arcam. (2014). Ti6Al4V Titanium Alloy, 4–6. https://doi.org/http://www.arcam.com/wp-content/uploads/Arcam-Ti6Al4V-Titanium-Alloy.pdf

Ataollahi Oshkour, A., Talebi, H., Seyed Shirazi, S. F., Bayat, M., Yau, Y. H., Tarlochan, F., & Abu Osman, N. A. (2014). Comparison of various functionally graded femoral prostheses by finite element analysis. *Scientific World Journal*, *2014*. https://doi.org/10.1155/2014/807621

Baharuddin, M. Y., Salleh, S.-H., Zulkifly, A. H., Lee, M. H., Noor, A. M., A Harris, A. R., … Abd Kader, A. S. (2014). Design process of cementless femoral stem using a nonlinear three dimensional finite element analysis. *BMC Musculoskeletal*

*Disorders*, *15*, 30. https://doi.org/10.1186/1471-2474-15-30

Bergmann, G., Deuretzbacher, G., Heller, M., Graichen, F., & Rohlmann, A. (2001). Hip contact and gait patterns from routine activities.PDF, *34*, 859–871. https://doi.org/10.1016/S0021-9290(01)00040-9

Biomet. (2012). Taperloc Complete Hip System Surgical Technique.

Brailovski, V., Jetté, B., Simoneau, C., Dumas, M., & Terriault, P. (2017). Femoral stem incorporating a diamond cubic lattice structure: Design, manufacture and testing. *Journal of the Mechanical Behavior of Biomedical Materials*, *77*(August 2017), 58–72. https://doi.org/10.1016/j.jmbbm.2017.08.034

Bruggi, M., & Taliercio, A. (2014). *Topology optimization for the development of eco-efficient masonry units*. *Eco-efficient Masonry Bricks and Blocks: Design, Properties and Durability*. Elsevier Ltd. https://doi.org/10.1016/B978-1-78242-305-8.00019-X

Chalernpon, K., Aroonjarattham, P., & Aroonjarattham, K. (2015). Static and Dynamic Load on Hip Contact of Hip Prosthesis and Thai Femoral Bones, *9*(3), 11–15.

Chang, C. L., Chen, C. S., Huang, C. H., & Hsu, M. L. (2012). Finite element analysis of the dental implant using a topology optimization method. *Medical Engineering and Physics*, *34*(7), 999–1008. https://doi.org/10.1016/j.medengphy.2012.06.004

Chen, J., Zhang, W. B., He, J. Z., Zhang, R., Cao, Y. Q., & Liu, X. (2018). Developmental dysplasia of the hip: A special pathology. *Chinese Journal of Traumatology - English Edition*, *21*(4), 238–242. https://doi.org/10.1016/j.cjtee.2018.02.001

Chen, W. C., Lai, Y. S., Cheng, C. K., & Chang, T. K. (2014). A cementless, proximally fixed anatomic femoral stem induces high micromotion with nontraumatic femoral

avascular necrosis: Afinite element study. *Journal of Orthopaedic Translation*, *2*(3), 149–156. https://doi.org/10.1016/j.jot.2014.03.002

Colic, K., Sedmak, A., Grbovic, A., Tatic, U., Sedmak, S., & Djordjevic, B. (2016). Finite element modeling of hip implant static loading. *Procedia Engineering*, *149*(June), 257–262. https://doi.org/10.1016/j.proeng.2016.06.664

Currey, J. A., Helms, J. A., Nanci, A., Guo, H., Wazen, R. M., & Brunski, J. B. (2013). Micromotion-induced strain fields influence early stages of repair at bone–implant interfaces. *Acta Biomaterialia*, *9*(5), 6663–6674. https://doi.org/10.1016/j.actbio.2013.01.014

Dayton, M. R., & Incavo, S. J. (2005). Component loosening in total hip arthroplasty. *Seminars in Arthroplasty*, *16*(2), 161–170. https://doi.org/10.1053/j.sart.2005.06.003

Doblaré, M., García, J. M., & Gómez, M. J. (2004). Modelling bone tissue fracture and healing: A review. *Engineering Fracture Mechanics*, *71*(13–14), 1809–1840. https://doi.org/10.1016/j.engfracmech.2003.08.003

Ebramzadeh, E., Sangiorgio, S. N., Longjohn, D. B., Buhari, C. F., & Dorr, L. D. (2004). Initial stability of cemented femoral stems as a function of surface finish, collar, and stem size. *The Journal of Bone and Joint Surgery. American Volume*, *86–A*(1), 106–115.

Energy, E. S. (n.d.). 5.2 Elastic Strain Energy. *Energy*, 180–193.

FDA approval for 3D printed titanium cranial plate. (2016). *Metal Powder Report*, *71*(4), 295. https://doi.org/10.1016/j.mprp.2016.04.014

FDA approval for 3D printed titanium implant. (2016). *Metal Powder Report*, *71*(5), 364. https://doi.org/10.1016/j.mprp.2016.08.067

G Robling, A., & H Turner, C. (2009). *Mechanical Signaling for Bone Modeling and Remodeling*. *Critical reviews in eukaryotic gene expression* (Vol. 19). https://doi.org/10.1615/CritRevEukarGeneExpr.v19.i4.50

Gardan, N., & Schneider, A. (2015). Topological optimization of internal patterns and support in additive manufacturing. *Journal of Manufacturing Systems*, *37*, 417–425. https://doi.org/10.1016/j.jmsy.2014.07.003

Gehrke, T., Citak, M., & Ohlmeier, M. (2019). Evolution of the cementless anatomic stem: Risks & rewards. *Seminars in Arthroplasty*. https://doi.org/10.1053/j.sart.2019.02.005

Grisez, B. T., Calkins, T. E., & Dietz, M. J. (2017). Modular Femoral Stems in Revision Total Hip Arthroplasty. *Operative Techniques in Orthopaedics*, *27*(3), 178–185. https://doi.org/10.1053/j.oto.2017.05.006

Harrysson, O. L. A., Cansizoglu, O., Marcellin-Little, D. J., Cormier, D. R., & West, H. A. (2008). Direct metal fabrication of titanium implants with tailored materials and mechanical properties using electron beam melting technology. *Materials Science and Engineering C*, *28*(3), 366–373. https://doi.org/10.1016/j.msec.2007.04.022

Hazlehurst, K. B. (2014). The Adoption of Laser Melting Technology for the Manufacture of Functionally Graded Cobalt Chrome Alloy Femoral Stems, 183.

Hazlehurst, K., Wang, C. J., & Stanford, M. (2013). Evaluation of the stiffness characteristics of square pore CoCrMo cellular structures manufactured using laser melting technology for potential orthopaedic applications. *Materials and Design*, *51*, 949–955. https://doi.org/10.1016/j.matdes.2013.05.009

Huiskes, R., Weinans, H., van Rietbergen, B., & Rietbergen, B. Van. (1992). The

relationship between stress shielding and bone resorption around total hip stems and the effects of flexible materials. *Clinical Orthopaedics and Related Research*, *NA;*(274), 124–134. https://doi.org/10.1097/00003086-199201000-00014

Jetté, B., Brailovski, V., Simoneau, C., Dumas, M., & Terriault, P. (2018). Development and in vitro validation of a simplified numerical model for the design of a biomimetic femoral stem. *Journal of the Mechanical Behavior of Biomedical Materials*, *77*(August 2017), 539–550. https://doi.org/10.1016/j.jmbbm.2017.10.019

Karuppal, R. (2016). Biological fixation of total hip arthroplasty: Facts and factors. *Journal of Orthopaedics*, *13*(3), 190–192. https://doi.org/10.1016/j.jor.2016.06.002

Kim, Y. H., Park, J. W., Kim, J. S., & Kim, I. W. (2016). Twenty-Five- to Twenty-Seven-Year Results of a Cemented vs a Cementless Stem in the Same Patients Younger Than 50 Years of Age. *Journal of Arthroplasty*, *31*(3), 662–667. https://doi.org/10.1016/j.arth.2015.09.045

Koenig, L., Feng, C., He, F., & Nguyen, J. T. (2018). The Effects of Revision Total Hip Arthroplasty on Medicare Spending and Beneficiary Outcomes: Implications for the Comprehensive Care for Joint Replacement Model. *Journal of Arthroplasty*, *33*(9), 2764–2769.e2. https://doi.org/10.1016/j.arth.2018.05.008

Lee, S.-H., Nomura, N., & Chiba, A. (2008). Significant Improvement in Mechanical Properties of Biomedical Co-Cr-Mo Alloys with Combination of N Addition and Cr-Enrichment. *Materials Transactions*, *49*(2), 260–264. https://doi.org/10.2320/matertrans.mra2007220

Li, X., Li, D., Lian, Q., Guo, H., & Jin, Z. (2010). *The Effect of Stem Structure on Stress*

*Distribution of a Custom-Made Hip Prosthesis*. *Proceedings of the Institution of Mechanical Engineers. Part H, Journal of engineering in medicine* (Vol. 224). https://doi.org/10.1243/09544119JEIM768

Li, X., Wang, C., Zhang, W., & Li, Y. (2009). Fabrication and characterization of porous Ti6Al4V parts for biomedical applications using electron beam melting process. *Materials Letters*, *63*(3–4), 403–405. https://doi.org/10.1016/j.matlet.2008.10.065

Limmahakhun, S., Oloyede, A., Chantarapanich, N., Jiamwatthanachai, P., Sitthiseripratip, K., Xiao, Y., & Yan, C. (2017). Alternative designs of load−sharing cobalt chromium graded femoral stems. *Materials Today Communications*, *12*(May), 1–10. https://doi.org/10.1016/j.mtcomm.2017.05.002

Mass, Y., & Amir, O. (2018). Using a virtual skeleton to increase printability of topology optimized design for industry-class applications. *Comptes Rendus - Mecanique*, *346*(11), 1104–1121. https://doi.org/10.1016/j.crme.2018.08.005

Mattei, L., Di Puccio, F., Piccigallo, B., & Ciulli, E. (2011). Lubrication and wear modelling of artificial hip joints: A review. *Tribology International*, *44*(5), 532–549. https://doi.org/10.1016/j.triboint.2010.06.010

Mirzendehdel, A. M., & Suresh, K. (2016). Support structure constrained topology optimization for additive manufacturing. *CAD Computer Aided Design*, *81*, 1–13. https://doi.org/10.1016/j.cad.2016.08.006

Nadeau, R. P., & Garbuz, D. S. (2016). Monoblock or modular tapered stems: Making the right choice. *Seminars in Arthroplasty*, *27*(4), 261–263. https://doi.org/10.1053/j.sart.2017.03.010

NJR. (2017). 14th Annual Report National Joint Registry for England, Wales, Northern

Ireland and the Isle of Man. *National Joint Registry*, *1821*(December 2016). https://doi.org/10.1038/nmat2505

Nuño, N., Groppetti, R., & Senin, N. (2006). Static coefficient of friction between stainless steel and PMMA used in cemented hip and knee implants. *Clinical Biomechanics*, *21*(9), 956–962. https://doi.org/10.1016/j.clinbiomech.2006.05.008

Ong, K. L., Lau, E., Suggs, J., Kurtz, S. M., & Manley, M. T. (2010). Risk of subsequent revision after primary and revision total joint arthroplasty. *Clinical Orthopaedics and Related Research*, *468*(11), 3070–3076. https://doi.org/10.1007/s11999-010-1399-0

Oshkour, A. A., Abu Osman, N. A., Davoodi, M. M., Yau, Y. H., Tarlochan, F., Wan Abas, W. A. B., & Bayat, M. (2013). Finite element analysis on longitudinal and radial functionally graded femoral prosthesis. *International Journal for Numerical Methods in Biomedical Engineering*, *29*(12), 1412–1427. https://doi.org/10.1002/cnm.2583

Oshkour, A. A., Talebi, H., Seyed Shirazi, S. F., Yau, Y. H., Tarlochan, F., & Abu Osman, N. A. (2015). Effect of Geometrical Parameters on the Performance of Longitudinal Functionally Graded Femoral Prostheses. *Artificial Organs*, *39*(2), 156–164. https://doi.org/10.1111/aor.12315

Ott, S. M. (2004). Bone Remodeling, Dynamics of. *Encyclopedia of Endocrine Diseases*, *1*, 386–391. https://doi.org/10.1016/b0-12-475570-4/00216-x

Park, J., & Sutradhar, A. (2015). A multi-resolution method for 3D multi-material topology optimization. *Computer Methods in Applied Mechanics and Engineering*, *285*, 571–586. https://doi.org/10.1016/j.cma.2014.10.011

Pasini, D., Tanzer, M., Rahimizadeh, A., Nourmohammadi, Z., & Arabnejad, S. (2017). Porous architected biomaterial for a tibial-knee implant with minimum bone resorption and bone-implant interface micromotion. *Journal of the Mechanical Behavior of Biomedical Materials*, *78*(November 2017), 465–479. https://doi.org/10.1016/j.jmbbm.2017.11.041

Perets, I., Chaharbakhshi, E. O., Mu, B., Ashberg, L., Battaglia, M. R., Yuen, L. C., & Domb, B. G. (2018). Hip Arthroscopy in Patients Ages 50 Years or Older: Minimum 5-Year Outcomes, Survivorship, and Risk Factors for Conversion to Total Hip Replacement. *Arthroscopy: The Journal of Arthroscopic & Related Surgery*, *34*(11), 3001–3009. https://doi.org/https://doi.org/10.1016/j.arthro.2018.05.034

Perrella, G., Fraldi, M., Esposito, L., Cowin, S. C., & Cutolo, A. (2009). Topological optimization in hip prosthesis design. *Biomechanics and Modeling in Mechanobiology*, *9*(4), 389–402. https://doi.org/10.1007/s10237-009-0183-0

Ramos, A., Completo, A., Relvas, C., & Simões, J. A. (2012). Design process of a novel cemented hip femoral stem concept. *Materials and Design*, *33*(1), 313–321. https://doi.org/10.1016/j.matdes.2011.07.039

Sandhu, H. S. (2015). Journey to total hip arthoplasty. *Journal of Arthroscopy and Joint Surgery*, *2*(1), 1–2. https://doi.org/10.1016/j.jajs.2014.12.007

Siva Rama Krishna, L., Mahesh, N., & Sateesh, N. (2017). Topology optimization using solid isotropic material with penalization technique for additive manufacturing. *Materials Today: Proceedings*, *4*(2), 1414–1422. https://doi.org/10.1016/j.matpr.2017.01.163

Stibolt, R. D., Patel, H. A., Huntley, S. R., Lehtonen, E. J., Shah, A. B., & Naranje, S.

M. (2018). Total hip arthroplasty for posttraumatic osteoarthritis following acetabular fracture: A systematic review of characteristics, outcomes, and complications. *Chinese Journal of Traumatology - English Edition*, *21*(3), 176–181. https://doi.org/10.1016/j.cjtee.2018.02.004

Takumi, W., Kazunori, Y., Jun Ichi, O., Taro, K., Seiryo, S., & Toshiaki, H. (2015). Ventricular fiber optimization utilizing the branching structure. *International Journal for Numerical Methods in Biomedical Engineering*, *32*(7), 1412–1427. https://doi.org/10.1002/cnm

Taniguchi, N., Fujibayashi, S., Takemoto, M., Sasaki, K., Otsuki, B., Nakamura, T., … Matsuda, S. (2016). Effect of pore size on bone ingrowth into porous titanium implants fabricated by additive manufacturing: An in vivo experiment. *Materials Science and Engineering C*, *59*, 690–701. https://doi.org/10.1016/j.msec.2015.10.069

Tian, X., Wang, Q., Liu, G., Liu, Y., Xie, Y., & Deng, W. (2019). Topology optimization design for offshore platform jacket structure. *Applied Ocean Research*, *84*(November 2018), 38–50. https://doi.org/10.1016/j.apor.2019.01.003

Vargas-Hernandez, J. S., Bingham, J. S., Hart, A., & Sierra, R. J. (2017). Cemented femoral stems: An invaluable solution. *Seminars in Arthroplasty*, *28*(4), 224–230. https://doi.org/10.1053/j.sart.2018.02.003

Vasista, S., & Tong, L. (2014). Topology optimisation via the moving iso-surface threshold method: Implementation and application. *Aeronautical Journal*, *118*(1201), 315–342. https://doi.org/10.1017/S0001924000009143

Veronese, N., & Maggi, S. (2018). Epidemiology and social costs of hip fracture. *Injury*, *49*(8), 1458–1460. https://doi.org/10.1016/j.injury.2018.04.015

Wang, S., Liu, T., Wang, Y., Yan, J., & Deng, X. (2015). Topology Optimization of Total Femur Structure: Application of Parameterized Level Set Method Under Geometric Constraints. *Journal of Mechanical Design*, *138*(1), 011402. https://doi.org/10.1115/1.4031803

Wang, X., Xu, S., Zhou, S., Xu, W., Leary, M., Choong, P., … Xie, Y. M. (2016). Topological design and additive manufacturing of porous metals for bone scaffolds and orthopaedic implants: A review. *Biomaterials*, *83*, 127–141. https://doi.org/10.1016/j.biomaterials.2016.01.012

What is an optimization process? (n.d.). Retrieved from https://abaqus-docs.mit.edu/2017/English/SIMACAECAERefMap/simacae-c-anaoptwhatis.htm

Yamako, G., Janssen, D., Hanada, S., Anijs, T., Ochiai, K., Totoribe, K., … Verdonschot, N. (2017). Improving stress shielding following total hip arthroplasty by using a femoral stem made of β type Ti-33.6Nb-4Sn with a Young's modulus gradation. *Journal of Biomechanics*, *63*, 135–143. https://doi.org/10.1016/j.jbiomech.2017.08.017

Zhang, K., Cheng, G., & Xu, L. (2019). Topology optimization considering overhang constraint in additive manufacturing. *Computers and Structures*, *212*, 86–100. https://doi.org/10.1016/j.compstruc.2018.10.011

Zhang, S., Le, C., Gain, A. L., & Norato, J. A. (2019). Fatigue-based topology optimization with non-proportional loads. *Computer Methods in Applied Mechanics and Engineering*, *345*, 805–825. https://doi.org/10.1016/j.cma.2018.11.015

Zhang, W., Zhou, Y., & Zhu, J. (2017). A comprehensive study of feature definitions with solids and voids for topology optimization. *Computer Methods in Applied*

*Mechanics and Engineering*, *325*, 289–313. https://doi.org/10.1016/j.cma.2017.07.004

Zimmer Biomet. (2019). Patient Matched Implant | Triflange Acetabular Component | Zimmer Biomet. Retrieved from https://www.zimmerbiomet.com/medical-professionals/hip/product/triflange-acetabular-component.html

# APPENDIX A: Material Models

Co-Cr-Mo:

| Strain | Stress |
|---|---|
| 0.000484 | 0 |
| 0.000531 | 57.21764 |
| 0.000591 | 151.4413 |
| 0.000645 | 241.0704 |
| 0.000732 | 401.9477 |
| 0.000786 | 507.6688 |
| 0.000833 | 565.1173 |
| 0.000974 | 611.026 |
| 0.001182 | 659.2011 |
| 0.001377 | 691.2907 |
| 0.001619 | 732.553 |
| 0.001908 | 773.7925 |
| 0.002143 | 803.5637 |
| 0.002378 | 826.4384 |
| 0.002647 | 856.1934 |
| 0.002909 | 881.3539 |
| 0.003467 | 922.4634 |
| 0.003809 | 942.9872 |
| 0.003185 | 904.2091 |
| 0.004045 | 961.2642 |

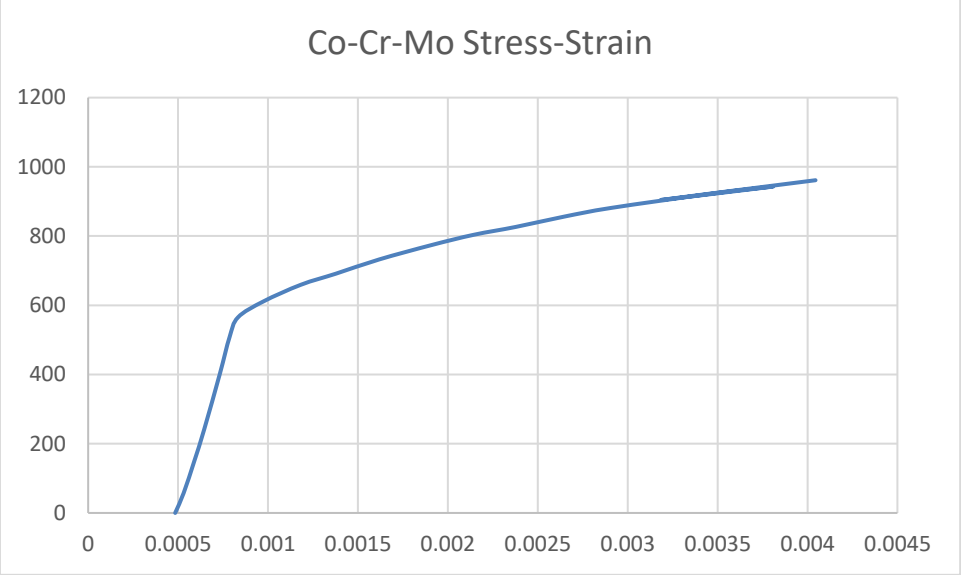


Ti-6Al-4V:

| Stress | Strain |
|---|---|
| 40 | 0 |
| 300 | 0.0025 |
| 650 | 0.005 |
| 1000 | 0.01 |
| 1120 | 0.02 |
| 1160 | 0.03 |
| 1165 | 0.04 |
| 1120 | 0.06 |
| 1040 | 0.08 |

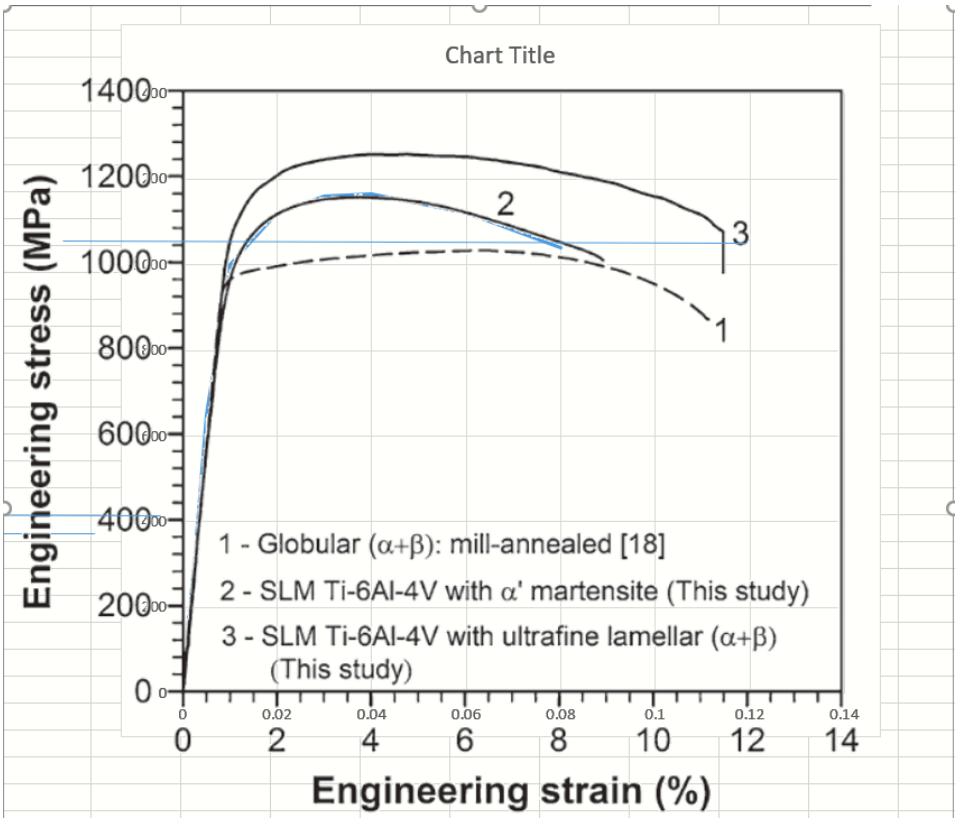


| Force | Displacement experimental |
|---|---|
| 0 | 0 |
| -300 | 0.70123 |
| -600 | 1.449953 |
| -900 | 2.251585 |
| -1200 | 3.111891 |
| -1500 | 4.037114 |
| -1800 | 5.034407 |
| -2100 | 6.112194 |
| -2400 | 7.280266 |

| | |
|---|---|
| -2700 | 8.550097 |
| -3000 | 9.93491 |

| Displacement Numerical | Force |
|---|---|
| 0 | 0 |
| 0.167457 | 69.87217 |
| 0.451817 | 181.6525 |
| 0.672986 | 253.5419 |
| 0.894155 | 341.3675 |
| 1.099526 | 413.2443 |
| 1.336493 | 493.1144 |
| 1.57346 | 565.0164 |
| 1.794629 | 644.8739 |
| 2.015798 | 724.7314 |
| 2.252765 | 796.6334 |
| 2.473934 | 868.5227 |
| 2.7109 | 956.361 |
| 2.916272 | 1028.238 |
| 3.137441 | 1116.063 |
| 3.374408 | 1195.933 |
| 3.579779 | 1259.842 |
| 3.816746 | 1347.68 |
| 4.06951 | 1419.595 |

| | |
|---|---|
| 4.259084 | 1491.459 |
| 4.496051 | 1563.361 |
| 4.71722 | 1627.282 |
| 4.985782 | 1699.209 |
| 5.206951 | 1771.099 |
| 5.443918 | 1827.065 |
| 5.680885 | 1898.967 |
| 5.902054 | 1970.856 |
| 6.139021 | 2026.822 |
| 6.391785 | 2098.736 |
| 6.597156 | 2178.581 |
| 6.818325 | 2258.439 |
| 7.07109 | 2330.353 |
| 7.292259 | 2394.274 |
| 7.513428 | 2466.164 |
| 7.766193 | 2538.078 |
| 7.987362 | 2594.031 |
| 8.208531 | 2649.985 |
| 8.477093 | 2705.975 |
| 8.729858 | 2769.922 |
| 8.982622 | 2801.996 |
| 9.235387 | 2834.07 |
| 9.503949 | 2898.029 |
| 9.709321 | 2969.906 |

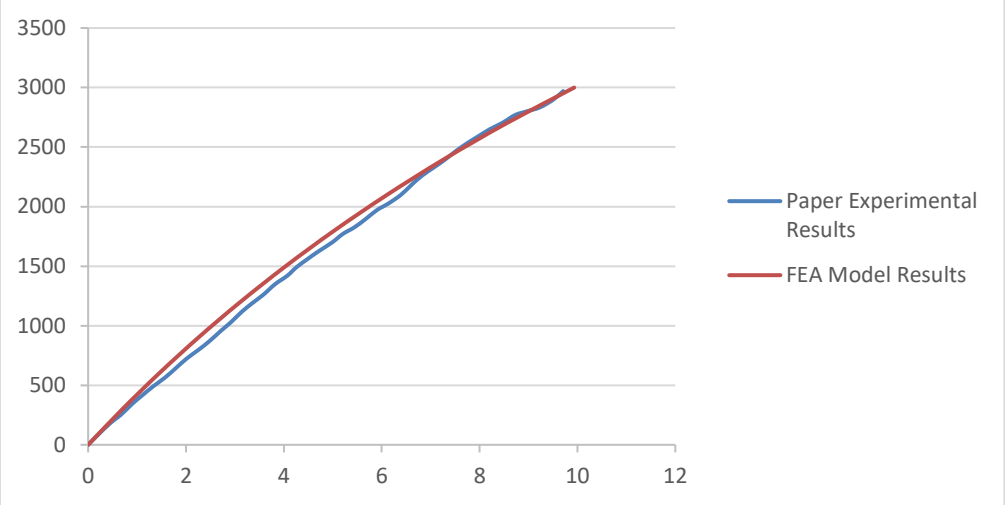
3500
3000
2500
2000
1500
1000
500
0
0
2
4
6
8
10
12
Paper Experimental Results
FEA Model Results